NASA TECHNICAL NOTE

NASA TN D-5637

NASA TN D-5637

c.1

INVESTIGATION OF LATERAL-DIRECTIONAL DYNAMIC STABILITY OF A TILT-WING V/STOL TRANSPORT

by Joseph R. Chambers and Sue B. Grafton

Langley Research Center
Langley Station, Hampton, Va.

NATIONAL AERONAUTICS AND SPACE ADMINISTRATION • WASHINGTON, D. C. • FEBRUARY 1970

1. Report No. NASA TN D-5637	2. Government Accession No.	3. Recipient's Catalog No.
4. Title and Subtitle INVESTIGATION OF LATERAL-DIRECTIONAL DYNAMIC STABILITY OF A TILT-WING V/STOL TRANSPORT		5. Report Date February 1970 6. Performing Organization Code
7. Author(s) Joseph R. Chambers and Sue B. Grafton		8. Performing Organization Report No. L-6848 10. Work Unit No. 721-05-10-01-23
9. Performing Organization Name and Address NASA Langley Research Center Hampton, Va. 23365		11. Contract or Grant No. 13. Type of Report and Period Covered Technical Note
12. Sponsoring Agency Name and Address National Aeronautics and Space Administration Washington, D.C. 20546		14. Sponsoring Agency Code

15. Supplementary Notes

16. Abstract

The investigation consisted of (1) static and dynamic force tests with a powered model to measure stability derivatives, (2) calculations of the lateral-directional dynamic stability characteristics, and (3) comparison of the calculated characteristics with current handling quality requirements for dynamic stability characteristics. The results indicated that the configuration would exhibit an unstable lateral-directional oscillation at low speeds. The dynamic stability characteristics of the basic airplane did not satisfy the handling quality requirements for wing-incidence angles greater than 30^{0}. The vehicle exhibited satisfactory characteristics when artificial stabilization was incorporated into the design.

17. Key Words Suggested by Author(s) Dynamic stability V/STOL airplane Stability derivatives	18. Distribution Statement Unclassified – Unlimited		
19. Security Classif. (of this report) Unclassified	20. Security Classif. (of this page) Unclassified	21. No. of Pages 51	22. Price* $3.00

*For sale by the Clearinghouse for Federal Scientific and Technical Information Springfield, Virginia 22151

INVESTIGATION OF LATERAL-DIRECTIONAL DYNAMIC STABILITY OF A TILT-WING V/STOL TRANSPORT

By Joseph R. Chambers and Sue B. Grafton
Langley Research Center

SUMMARY

An investigation was conducted to determine the lateral-directional dynamic stability characteristics of a tilt-wing V/STOL transport. The investigation consisted of (1) static and dynamic force tests with a powered model to measure stability derivatives, (2) calculations of the lateral-directional dynamic stability characteristics, and (3) comparison of the calculated characteristics with current handling quality requirements for dynamic stability characteristics.

The results of the force tests indicate large effects of power on the static and dynamic stability derivatives for this type of airplane. The results of the calculations indicate that the control-fixed motions of the airplane without artificial stabilization in hovering flight would be dominated by an unstable oscillation involving roll-angle and sideward translation. As the transition to forward flight progressed, the oscillation became less unstable and became the classical Dutch roll oscillation in conventional flight. The results of the calculations also indicated that the unstable oscillation which occurred at low speeds could be stabilized by the addition of roll-rate and roll-attitude stabilization. The dynamic stability characteristics of the basic unaugmented airplane did not satisfy current handling quality requirements for wing-incidence angles greater than 30°. The addition of sufficient artificial stabilization to insure compliance with dynamic stability requirements in hovering flight also satisfied requirements for dynamic stability at higher speeds.

INTRODUCTION

The National Aeronautics and Space Administration has conducted several investigations in the past to provide basic information relating to the dynamic stability and control characteristics of tilt-wing V/STOL transports. (For examples, see refs. 1 to 5.) Although the lateral-directional flying qualities of tilt-wing airplanes have been evaluated during the course of previous investigations, the basic factors affecting the dynamic stability characteristics of this class of airplane are not well-known. This situation has been brought about primarily by the lack of reliable values of stability derivatives for

V/STOL airplanes. The present study was therefore undertaken to measure the static and dynamic derivatives and to define the general nature of the lateral-directional dynamic stability characteristics of a tilt-wing V/STOL transport.

The investigation was conducted in three phases. In the first phase, static and forced-oscillation tests were conducted with a powered 1/9-scale model of a four-propeller V/STOL transport in order to measure representative values of the static and dynamic lateral-directional stability derivatives. The second phase of the investigation was an analytical study in which the measured aerodynamic derivatives were used to calculate the lateral-directional dynamic stability characteristics of a full-scale vehicle from hovering to conventional forward flight. These calculated characteristics were correlated with qualitative evaluations of the lateral-directional characteristics displayed by the model during free-flight tests. In the third phase of the investigation, an effort was made to determine the effect of the calculated lateral-directional dynamic stability characteristics on flying qualities based on current handling quality requirements.

SYMBOLS

All quantities are presented with respect to the system of body axes shown in figure 1. When flight velocities approach zero, the conventional nondimensional coefficients lose significance and tend to become infinite. Data presented herein are therefore given in both dimensional and nondimensional form. Dimensional values of the physical quantities are given both in the U.S. Customary Units and in the International System of Units (SI).

A,B,C,D,E	coefficients of quartic equation defined in appendix A
b	wing span, ft (m)
C_L	lift coefficient, $F_L/q_\infty S$
C_l	rolling-moment coefficient, $M_X/q_\infty Sb$
C_n	yawing-moment coefficient, $M_Z/q_\infty Sb$
C_Y	side-force coefficient, $F_Y/q_\infty S$
$C_{1/2}$	cycles required for oscillation to damp to one-half amplitude
C_2	cycles required for oscillation to double amplitude

$\bar{c}$ mean aerodynamic chord, ft (m)

E strain-gage supply voltage, volts

E_{in} voltage in phase with displacement, volts

E_{out} voltage out of phase with displacement, volts

E_R amplitude of resolver voltage, volts

e_ℓ voltage proportional to rolling moment, volts

e_n voltage proportional to yawing moment, volts

e_y voltage proportional to side force, volts

F_L lift, lb (N)

$F_{L,o}$ lift for hovering flight, lb (N)

F_X force along X body axis, lb (N)

F_Y force along Y body axis, lb (N)

f frequency of oscillation, cycles per second

g acceleration due to gravity, ft/sec^2 (m/sec^2)

I_X moment of inertia about X body axis, slug-ft^2 (kg-m^2)

I_Z moment of inertia about Z body axis, slug-ft^2 (kg-m^2)

i_t tail incidence, deg

i_w wing incidence, deg

$j = \sqrt{-1}$

$K_\ell = E_R k_\ell E$

k_l	balance calibration factor, volts/volt-ft-lb (volts/volt-m-N)
M_X	rolling moment, ft-lb (m-N)
$M_{X,st}$	static rolling moment, ft-lb (m-N)
M_Z	yawing moment, ft-lb (m-N)
m	mass, slugs (kg)
P	period of oscillation, sec
p	rolling velocity, rad/sec
q_∞	free-stream dynamic pressure, lb/ft^2 (N/m^2)
r	yawing velocity, rad/sec
S	wing area, ft^2 (m^2)
s	Laplace operator, $\sigma + j\omega$, 1/sec
T	period of oscillation of forced-oscillation tests, sec
t	time, sec
t_o	reference time, sec
$t_{1/2}$	time required for a mode of motion to damp to one-half amplitude, sec
t_2	time required for a mode of motion to double amplitude, sec
V	free-stream velocity, ft/sec (m/sec) or knots
v	pertubation velocity along Y body axis, ft/sec (m/sec)
v_e	equivalent side velocity, $v\sqrt{\sigma}$, ft/sec (m/sec)
W	gross weight of airplane, lb (N)

W/S	wing loading, lb/ft^2 (N/m^2)
X,Y,Z	body reference axes (see fig. 1)
α	angle of attack, deg or rad
β	angle of sideslip, deg or rad
γ	flight-path angle, positive for climb, deg
ζ	ratio of damping present in oscillatory mode of motion to value required for critical damping
ϕ	angle of bank, deg or rad
$\Delta\phi_{max}$	amplitude of incremental bank angle during oscillation, deg or rad
σ	real part of root of characteristic equation, 1/sec; ratio of air density at altitude to air density at sea level
ψ	angle of yaw, rad
$\left\lvert\frac{\phi}{v_e}\right\rvert$	ratio of bank-angle amplitude to equivalent-side-velocity amplitude for oscillatory mode, $\left\lvert\frac{\phi}{\beta}\right\rvert\frac{57.3}{V\sqrt{\sigma}}, \frac{deg}{ft/sec}$ $\left(\frac{deg}{m/sec}\right)$
$\left\lvert\frac{\phi}{\psi}\right\rvert$	ratio of amplitudes of roll and yaw present in an oscillatory mode of motion
$\left\lvert\frac{\phi}{\beta}\right\rvert$	ratio of amplitudes of roll and sideslip present in an oscillatory mode of motion
ω	imaginary part of root of characteristic equation, 1/sec; also oscillatory frequency ($\omega = 2\pi f$), rad/sec
ω_d	damped frequency of oscillatory mode of motion, rad/sec
ω_n	undamped natural frequency of oscillatory mode of motion, rad/sec

Nondimensional stability derivatives (β in radians):

$$C_{L_\alpha} = \frac{\partial C_L}{\partial \alpha}$$

$$C_{l_p} = \frac{\partial C_l}{\partial \frac{pb}{2V}} \qquad C_{n_p} = \frac{\partial C_n}{\partial \frac{pb}{2V}} \qquad C_{Y_p} = \frac{\partial C_Y}{\partial \frac{pb}{2V}}$$

$$C_{l_r} = \frac{\partial C_l}{\partial \frac{rb}{2V}} \qquad C_{n_r} = \frac{\partial C_n}{\partial \frac{rb}{2V}} \qquad C_{Y_r} = \frac{\partial C_Y}{\partial \frac{rb}{2V}}$$

$$C_{l_\beta} = \frac{\partial C_l}{\partial \beta} \qquad C_{n_\beta} = \frac{\partial C_n}{\partial \beta} \qquad C_{Y_\beta} = \frac{\partial C_Y}{\partial \beta}$$

$$C_{l_{\dot\beta}} = \frac{\partial C_l}{\partial \frac{\dot\beta b}{2V}} \qquad C_{n_{\dot\beta}} = \frac{\partial C_n}{\partial \frac{\dot\beta b}{2V}} \qquad C_{Y_{\dot\beta}} = \frac{\partial C_Y}{\partial \frac{\dot\beta b}{2V}}$$

$$C_{l_{\dot p}} = \frac{\partial C_l}{\partial \frac{\dot p b^2}{4V^2}}$$

Dimensional stability derivatives:

$$L_v = \frac{1}{I_X}\frac{\partial M_X}{\partial v} \qquad N_v = \frac{1}{I_Z}\frac{\partial M_Z}{\partial v} \qquad M_{X_p} = \frac{\partial M_X}{\partial p} \qquad Y_v = \frac{1}{m}\frac{\partial F_Y}{\partial v}$$

$$L_p = \frac{1}{I_X}\frac{\partial M_X}{\partial p} \qquad N_p = \frac{1}{I_Z}\frac{\partial M_Z}{\partial p} \qquad M_{X_{\dot p}} = \frac{\partial M_X}{\partial \dot p} \qquad Y_p = \frac{1}{m}\frac{\partial F_Y}{\partial p}$$

$$L_r = \frac{1}{I_X}\frac{\partial M_X}{\partial r} \qquad N_r = \frac{1}{I_Z}\frac{\partial M_Z}{\partial r} \qquad M_{X_\beta} = \frac{\partial M_X}{\partial \beta} \qquad Y_r = \frac{1}{m}\frac{\partial F_Y}{\partial r}$$

$$L_\beta = \frac{1}{I_X}\frac{\partial M_X}{\partial \beta} \qquad N_\beta = \frac{1}{I_Z}\frac{\partial M_Z}{\partial \beta} \qquad M_{X_{\dot\beta}} = \frac{\partial M_X}{\partial \dot\beta}$$

$$L_\phi = \frac{1}{I_X}\frac{\partial M_X}{\partial \phi}$$

A dot over a symbol represents a derivative with respect to time. A bar over a symbol represents an average value.

DESCRIPTION OF AIRPLANE

Although wind-tunnel tests were made on a model, the analysis was made for the full-scale airplane. The airplane configuration was the four-propeller, tilt-wing V/STOL transport shown in the three-view sketch presented in figure 2. Mass and dimensional characteristics of the airplane are listed in table I. The airplane employed a full-span double-slotted flap and an all-movable horizontal tail. The flap and the tail were programed to deflect with variations of wing-incidence angles to minimize wing stall and longitudinal trim changes through the transition from hovering to conventional forward flight. The programed variations of flap-deflection angle and horizontal-tail incidence for the present study are shown in figure 3; these variations are identical to those used for the free-flight model tests of reference 1. The horizontal and vertical locations of the center of gravity of the vehicle were assumed to vary with wing-incidence angle in the same manner as noted in reference 1; these variations are presented in figure 4.

MODEL, APPARATUS, AND TESTING PROCEDURE

The 1/9-scale powered free-flight model of reference 1 was used to obtain values of the static and dynamic lateral-directional stability derivatives used in the investigation. Although theoretical estimates of stability derivatives were available, values of derivatives obtained from powered model tests were believed to be far more accurate and representative than theoretical estimates because of the large effects of power on the stability derivatives (ref. 4).

Tunnel

All tests were conducted in the open-throat test section of the Langley full-scale tunnel with the model moment-reference center about 7 feet (2.14 m) above the ground board. The effects of flow angularity and blockage were negligible for the present study; therefore, no corrections have been applied to the data.

Model

A photograph of the 1/9-scale tilt-wing transport model used for the force tests is presented in figure 5. The four main propellers were interconnected by a system of shafts and gearboxes to insure synchronization of the propulsion system. Because the main propellers rotated in opposite directions for each wing panel (fig. 2), the gyroscopic effects associated with the propellers were eliminated. Two pneumatic motors driven by

compressed air powered the main propellers and tail rotor. An electric motor provided remote actuation of the wing-incidence angle which ranged from $i_w = 0^o$ (wing positioned for conventional forward flight) to $i_w = 90^o$ (wing positioned for vertical or hovering flight). Additional information relating to the model can be found in reference 1.

Apparatus

All tests were made with a sting or single-strut support system and a six-component internal strain-gage balance. The static force tests were made with the model sting-mounted through the rear of the fuselage; the forced-oscillation tests were made by using the technique sketched in figure 6. During the forced-oscillation tests, the model was mounted with its wings in a vertical plane. For the forced-oscillation tests in roll (fig. 6(a)), the balance was attached directly to the end of the sting and was alined with the longitudinal axis of the model. A bellcrank-pushrod assembly forced the model to oscillate at a fixed frequency and amplitude. The system was powered by a 3-horsepower (2.2 kW) variable-speed electric motor and flywheel mounted directly on the vertical support column. The frequency of the oscillatory motion was varied by changing the frequency of the input electric power to the electric motor.

A precision sine-cosine potentiometer, which was mounted on the flywheel, generated voltage signals proportional to the sine and cosine of the flywheel rotation angle and produced voltages proportional to the angular displacement and angular velocity of the model. These signals were used in the data-reduction procedure described in appendix B of this report.

The compressed air power for the pneumatic motors was supplied through flexible plastic tubing. The air supply was varied remotely and frequency meters were monitored to maintain constant propeller rotational speed during the tests. Angle of attack was varied by rotating the vertical support column, which was mounted on a motor-driven turntable.

For the forced-oscillation tests in yaw (fig. 6(b)), the model and balance were reoriented so that the sting entered the bottom of the model along the Z body axis and produced yawing motions.

TESTS

The static and dynamic force tests were made for wing-incidence angles ranging from 0^o to 70^o in increments of 10^o. In addition, tests were made with $i_w = 90^o$ and the model at 90^o sideslip to determine the lateral-directional stability derivatives of the configuration in hovering flight. The static force tests were made for sideslip angles ranging from -20^o to 20^o; and the forced-oscillation tests were made for an oscillation

amplitude of $\pm 5^{\circ}$. All dynamic tests were conducted at a frequency of 1 cycle per second. During all tests, the main propeller blades were set at an angle of 12° at the 0.75-radius position. The tail rotor was operated with the blades set at 0° pitch. The test procedure is described in detail in reference 4.

Although the primary purpose of the force tests was to determine the lateral-directional stability derivatives for trimmed level flight at $\alpha = 0^{\circ}$, additional tests were made to evaluate the effects of reduced power (simulating decelerating or descending flight) on the values of the derivatives.

All force test data were obtained for the moment-reference-center location shown in figure 2. The measured values were transferred to the center-of-gravity position of the airplane (fig. 4) by the equations presented in reference 6.

CALCULATIONS

Calculations were made to determine the lateral-directional dynamic stability characteristics of the vehicle for level flight at various wing-incidence angles used during the force tests. These calculations determined the stability of the airplane at a given wing-incidence angle and flight condition; therefore, the stability derivatives were not considered to be functions of time as they would be for a rapid transition to forward flight. The calculations employed the linearized equations of motion presented in appendix A. The results of the calculations were the period P, time to half amplitude $t_{1/2}$, natural frequency ω_n, damping ratio ζ, and the magnitude and phase relationship of roll-sideslip $|\phi/\beta|$ and roll-yaw $|\phi/\psi|$ ratios. In conjunction with the calculations, the root-locus technique was used to illustrate graphically the change in stability of the vehicle at various stages of the flight range.

RESULTS OF FORCE TESTS

The results of the static and forced-oscillation tests conducted with the 1/9-scale model are presented in figures 7 to 10. These data were obtained for level flight at an angle of attack of 0° and are presented with respect to the moment-reference-center location given in figure 2.

Results of Static Force Tests

The variations of the static lateral-directional force and moment coefficients with sideslip angle are presented in figure 7. The model exhibited positive effective dihedral $\left(\text{negative values of } C_{l_\beta}\right)$ and positive directional stability $\left(\text{positive values of } C_{n_\beta}\right)$ for all wing-incidence angles that were studied. The data are generally linear with respect

to sideslip angle with the exception of the yawing-moment coefficient C_n which indicates a reduction in directional stability as angle of sideslip is increased.

The linearized values of the static stability derivatives, based on the values of the coefficients at $\beta = \pm 5^o$, are presented in figure 8. The value of the side-force derivative for $i_w = 0^o$ is quite large $\left(C_{Y_\beta} = -1.73\right)$. In comparison, most present-day subsonic jet transports have values of C_{Y_β} about one-half as large as that of the test configuration. Examination of limited longitudinal data obtained during the present study and additional data presented in reference 3 indicated that the value of C_{Y_β} was about one-third the value of the slope of the lift curve C_{L_α}. This result indicates that the tilt-wing V/STOL airplane would be more sensitive to sidewinds than conventional airplanes and would experience lateral accelerations due to side gusts about one-third as great as the normal accelerations due to vertical gusts. These lateral accelerations would be considered to be especially uncomfortable, based on the well-known fact that pilots are less tolerable of lateral accelerations than normal accelerations. Therefore, these side-force characteristics would be expected to result in poor riding qualities. Another point to be noted in figure 8 is the low value of the directional stability derivative for $i_w = 0^o$ $\left(C_{n_\beta} = 0.054\right)$. This level of directional stability is about one-half as large as that exhibited by subsonic jet transports.

The variations of the lateral-directional forces and moments with lateral velocity for the hovering configuration $\left(i_w = 90^o\right)$ as presented in figure 9 were scaled by the relations given in reference 5. For positive lateral velocities, the model had stabilizing dihedral effect (negative variation of $M_X/F_{L,o}b$ with lateral velocity). The model had essentially neutral directional stability (no variation of $M_Z/F_{L,o}b$ with lateral velocity) for values of side velocity up to about 15 ft/sec (5 m/sec).

Results of Forced-Oscillation Tests

The results of the forced-oscillation tests in yaw are presented in figure 10(a). The aerodynamic data obtained are combinations of derivatives due to yaw rate r and side acceleration $\dot{\beta}$. The derivatives were obtained in combination because the model was oscillated in yaw at zero angle of attack; oscillation under these conditions resulted in changes in both yaw rate and angle of sideslip. Figure 10(a) indicates that the model had positive damping in yaw $\left(\text{negative values of } C_{n_r} - C_{n_{\dot{\beta}}}\right)$ for all values of wing incidence. The magnitude of the damping in yaw for $i_w = 0^o$ $\left(C_{n_r} - C_{n_{\dot{\beta}}} = -0.735\right)$ indicates a large effect of the propellers inasmuch as an estimate of the power-off value of this parameter is about -0.15. The rolling moment due to yaw rate $\left(C_{l_r} - C_{l_{\dot{\beta}}}\right)$ remained positive over the range of i_w; whereas the side force due to yaw rate $\left(C_{Y_r} - C_{Y_{\dot{\beta}}}\right)$ was

positive for value of i_w less than 47^o but changed to negative for values of i_w greater than 47^o.

The results of the forced-oscillation tests in roll are presented in figure 10(b). Because the tests were conducted at an angle of attack of 0^o, no sideslip was generated, and the measured aerodynamic derivatives are therefore due only to roll rate p. The data of figure 10(b) indicate that the model had positive damping in roll (negative values of C_{l_p}) for all values of wing incidence. The value of C_{l_p} for cruising flight ($i_w = 0^o$) is quite large ($C_{l_p} = -0.73$) in comparison with the power-off contribution of the wing to C_{l_p}, which should be about -0.4. The comparison indicates a large contribution of the propellers and power effects to the damping-in-roll derivative. This contribution should be considered in estimations of stability derivatives for this type of airplane. In addition, the data of figure 10(b) show that the value of the yawing moment due to roll rate C_{n_p} is negative for most of the range of wing-incidence angle. Experience with conventional airplanes has shown that negative values of C_{n_p} are usually detrimental to both dynamic stability and control.

Effects of Power on Stability Derivatives

As mentioned earlier, the primary goal of the first phase of the investigation was to measure static and dynamic lateral-directional stability derivatives for trimmed level flight. Additional tests were conducted to gain some insight into the effect of power condition on the values of the static and dynamic derivatives. The results of the tests, which were conducted for a wing-incidence angle of 30^o and an angle of attack of 0^o, are presented in figure 11. The variations of the rolling, yawing, and sideslip derivatives with power condition are shown. Because the model was not instrumented for propeller thrust measurements, the power condition is referenced by the flight-path angle γ $\left(\tan^{-1}\frac{F_X}{F_L}\right)$. Increasing negative values for γ correspond to an increase in descent angle or a reduction in power. The data for $i_w = 30^o$ show that reduction in power from that required for level flight ($\gamma = 0^o$) caused large decreases in the magnitudes of the static and dynamic stability derivatives. For example, when the descent angle was increased to 10^o ($\gamma = -10^o$), the damping-in-yaw parameter $C_{n_r} - C_{n_{\dot{\beta}}}$ was reduced by 16 percent, the damping-in-roll derivative C_{l_p} was reduced by 43 percent, and the directional stability derivative C_{n_β} was reduced by 40 percent. These data illustrate the significant effects of power condition on the static and dynamic stability derivatives of tilt-wing airplanes.

Up to the present time, the primary reason for the deterioration of lateral-directional handling qualities of tilt-wing airplanes in descending flight has been accepted to be disturbances caused by flow separation. The data of figure 11, however, indicate

that significant reductions of aerodynamic damping also occur in descent, which would be expected to increase the airplane response to stall-induced disturbances and thereby compound an already difficult piloting task.

Aerodynamic Characteristics of the Full-Scale Airplane

The results presented in figures 8 to 10 were used to calculate static and dynamic stability derivatives for the full-scale airplane, which was assumed to have a wing loading of 70 lb/ft^2 (3350 N/m^2). Based on longitudinal data obtained with the model of the present investigation, figure 12 shows the variation of trim velocity with wing-incidence angle. The experimental values of the static and dynamic stability derivatives were transferred to the center-of-gravity positions given in figure 4 and were then dimensionalized by using appropriate dimensional and aerodynamic constants. Dimensional interpretation is desirable because conventional nondimensional derivatives have infinite values at zero airspeed. The dimensional stability derivatives for the full-scale airplane are presented in figure 13 and in table II.

RESULTS OF CALCULATIONS

The aerodynamic data previously discussed were used to calculate the dynamic stability characteristics of the full-scale airplane from hovering to conventional forward flight. The results of the calculations are presented in figures 14 to 16 and in table III. The calculated results for hovering flight and transition flight are discussed individually.

Hovering Flight

Basic airplane.- The results of the calculations for hovering flight ($i_W = 90^o$), which are listed in table III, indicate that the uncontrolled (control-fixed) motions of the basic airplane without stability augmentation would consist of two aperiodic stable modes of motion and an unstable oscillation. After an external disturbance in hovering flight, the two stable modes rapidly subside, while the magnitude of the divergent oscillation increases and soon dominates the vehicle response. An unstable oscillation during hovering flight is a well-documented characteristic of the helicopter and of propeller- and fan-powered V/STOL configurations. Examination of the relative magnitudes of the terms in the equations of motion indicates that the unstable oscillation is produced by lack of adequate aerodynamic damping in roll L_p and by excessive values of rolling moment due to side velocity L_v in hovering flight. Increases in the values of moment due to speed perturbations tend to make the vehicle more unstable, whereas, increases in aerodynamic damping tend to stabilize the vehicle.

Effect of stability augmentation.- The fact that increases in L_p will stabilize the oscillation in hovering flight can be utilized in the design of stability augmentation systems

for V/STOL airplanes. Insuring satisfactory flying qualities, however, usually involves more than simple roll-rate augmentation. As roll damping is increased, the control inputs decrease in effectiveness. Therefore, the pilot must combat sluggish maneuverability as well as control the attitude of the vehicle, a difficult task in gusty wind.

One scheme for stabilizing the vehicle while maintaining acceptable response characteristics and reducing the workload associated with attitude control requires the addition of roll-attitude stabilization L_ϕ. The effects of increases in L_p and L_ϕ are illustrated in the root-locus sketch in figure 14. The darkened circular symbols represent the complex roots of the unstable oscillation for the basic configuration in hovering flight. The roots are located in the right, or unstable, half of the complex plane. Addition of roll-rate augmentation is indicated by the locus of roots denoted by square symbols. As the figure shows, the unstable roots can be made stable (moved to the left half of the complex plane) by the addition of L_p. On the other hand, addition of only roll-attitude stabilization L_ϕ results primarily in an increase in frequency of the oscillation. The simultaneous addition of both rate and attitude stabilization can produce any desired level of stability and frequency. Experience has shown that relatively high gains are required and that artificial damping in yaw will be needed for adequate flying qualities in hovering flight. A typical augmentation system would produce values of L_p, L_ϕ, and N_r equal to about -4.0, which would lead to virtually deadbeat damping of the oscillatory mode.

Transition Flight

Basic airplane.- The results presented in table III show that as the transition from hovering to conventional forward flight progresses, the unstable oscillation of hovering flight becomes less unstable. At an airspeed of about 30 knots $(i_w \approx 55^o)$, the airplane becomes dynamically stable. The variation of stability with increasing airspeed is illustrated in figure 15, which shows the location of roots as a function of wing incidence. As wing incidence is reduced from 90^o and forward speed is increased, the unstable oscillation becomes less unstable and gradually becomes the classical Dutch roll oscillation in conventional forward flight. The aperiodic modes of hovering flight become the conventional roll-subsidence mode and spiral mode in cruising flight. The Dutch roll oscillation for $i_w = 0^o$ is heavily damped ($\zeta = 0.7$) because of the relatively large magnitudes of L_p and N_r in conventional flight.

The nature of the stability of the airplane in the transition speed range is illustrated by the calculated time histories of figure 16, which presents motions of the test vehicle after release from an initial sideslip angle of 5^o at wing-incidence angles of 0^o, 30^o, and 70^o. The response of the vehicle for $i_w = 70^o$ is quite unstable and is very similar to the response in hovering flight. When the wing incidence is reduced to 30^o (with a

corresponding increase in trim speed), the response is dynamically stable although lightly damped. Further reduction of i_w to 0^o results in almost deadbeat damping, as anticipated in the previous discussion. The progression of dynamic stability characteristics from those of a dynamically unstable vehicle in hovering flight to those of a dynamically stable vehicle in forward flight is caused by increase in natural aerodynamic damping due to increased effectiveness of the aerodynamic surfaces and changes in airplane configuration as airspeed is increased.

Effect of stability augmentation.- The calculated results indicate that some form of stability augmentation, preferably a combination of rate and attitude augmentation, is required to insure adequate flying qualities in low-speed flight. Because the dynamic instability is greatest in hovering flight, it might be expected that levels of artificial stabilization which are adequate for hovering flight will be sufficient for the transition speed range. Calculations were made which assumed that the values of N_r, L_p, and L_ϕ were maintained at a constant value of -4.0 throughout the transition. These unpublished results indicate that all modes of motion would be aperiodic and stable and would thereby insure deadbeat damping. In this case, the gain of the stability augmentation system is usually a function of wing-incidence angle so that the augmentation is phased out as the cruise configuration is approached.

CORRELATION WITH MODEL FREE-FLIGHT TESTS

The model used in the measurement of stability derivatives had previously undergone a series of free-flight tests during which qualitative measurements were made of the control-fixed characteristics of lateral-directional dynamic stability. The dynamic stability measurements consisted of motion-picture records of control-fixed motions following control inputs from trim flight conditions. A description of the free-flight technique and tests is presented in reference 1. A photograph of the model in free flight in the Langley full-scale tunnel is presented in figure 17.

The flight tests to determine the basic stability of the model in hovering flight showed that the model had an unstable control-fixed oscillation similar to the oscillation calculated in the previous section. An example of the motions encountered in roll and sideward translation for hovering flight are presented in figure 18. Unfortunately, the motions are so unstable that a direct comparison of the period and time to double amplitude is not possible; but the general nature of the response, including phasing of roll angle and sideways displacement, agrees with the calculated results.

In the transition flight range, the model exhibited no significant oscillatory instability for wing-incidence angles less than $i_w = 70^o$. Instead, the model performed a slow sidewise divergence with little yawing. The calculated results presented in table III indicate

neutral oscillatory stability $\left(t_{1/2} = \infty\right)$ between $i_w = 50^o$ and $i_w = 60^o$ instead of at $i_w = 70^o$ and no tendency toward sidewise divergence. These apparent discrepancies might have been caused by (1) difficulty associated with trimming the model and defining the exact point at which neutral oscillatory stability occurs during free-flight tests and by (2) modifications to the configuration which may have produced significant changes in the stability derivatives of the model. The model configuration as flown in the tests of reference 1 exhibited neutral directional stability for small sideslip angles; whereas, for the present force tests, various geometric modifications, including fillets and sealed fuselage-flap juncture, were incorporated to eliminate the small region of neutral stability which was found to be unrepresentative of the full-scale vehicle based on tests of several other models of the same configuration.

COMPARISON WITH HANDLING QUALITY SPECIFICATIONS

The results of the preceding calculations have been compared with several current handling quality requirements in an effort to determine the effects of the dynamic-stability requirements on flying qualities. It should be noted that several factors other than dynamic stability (such as aircraft response to control inputs) can have significant effects on handling qualities; therefore, compliance with the following specifications is only one of several conditions which must be satisfied for adequate flying qualities. The results are compared with specifications for helicopters, conventional airplanes, and V/STOL airplanes.

The results of the calculations are compared with the current military specification for helicopters (ref. 7) in figure 19(a). The hatched boundary in figure 19(a) represents the minimum requirement for all-weather and instrument flight conditions. These data indicate that the tilt-wing airplane does not meet the specifications for wing-incidence angles greater than 30^o.

The characteristics of the test airplane are compared with the specifications for manned military airplanes (ref. 8) in figure 19(b). The hatched boundary defines those conditions considered to be unsatisfactory for normal operations without stability augmentation. Again, the present configuration does not meet the requirements for wing-incidence values greater than $i_w = 30^o$.

A generally accepted criterion for V/STOL aircraft handling quality requirements has been stated in reference 9. The characteristics of the test configuration are compared with this criterion in figure 19(c). Boundaries are indicated for normal operation and for flight with single failure of the stability augmentation system. As the figure shows, the current test vehicle does not satisfy the normal-operations requirement for wing-incidence angles greater than 30^o.

Apparently, the basic airplane without artificial stability augmentation will satisfy all three specifications for wing-incidence angles less than about 30°, but it will not satisfy any of these specifications for wing-incidence angles greater than about 30°. Therefore, stability augmentation must be provided for satisfactory compliance with the specifications. If stability augmentation were added to insure compliance with dynamic stability requirements in hovering flight, the airplane would meet all of the preceding requirements for flight at higher speeds.

SUMMARY OF RESULTS

The results of an investigation to determine the lateral-directional dynamic stability characteristics of a tilt-wing V/STOL transport may be summarized as follows:

1. Large effects of power on the values of the static and dynamic stability derivatives are to be expected for this type of airplane.

2. In hovering flight, the control-fixed motion of the airplane without artificial stabilization will be dominated by an unstable oscillation involving roll angle and sideward translation.

3. As the transition to forward flight progresses, the oscillation becomes less unstable and becomes the classical Dutch roll oscillation in conventional flight.

4. The unstable oscillation which occurs at low speeds may be stabilized to almost any desired degree by the simultaneous addition of roll-rate and roll-attitude stabilization.

5. The dynamic stability characteristics of the basic unaugmented airplane did not satisfy current handling quality requirements for dynamic stability for wing-incidence angles greater than 30°.

6. The results of the calculations indicated that the addition of sufficient artificial stabilization to insure satisfactory dynamic stability characteristics in hovering flight also would insure compliance with the dynamic stability requirements at higher speeds.

Langley Research Center,
National Aeronautics and Space Administration,
Langley Station, Hampton, Va., November 20, 1969.

APPENDIX A

EQUATIONS OF MOTION

The linearized, small-perturbation equations of motion for fuselage-level horizontal flight referred to a body system of axes (fig. 1) may be expressed as follows:

Side force:

$$\left(s - Y_v\right)\beta + \left(-sY_p - \frac{g}{V}\right)\phi + \left(-Y_r + 1\right)r = 0 \tag{A1}$$

Rolling moment:

$$-L_\beta\beta + \left(s^2 - sL_p\right)\phi - L_r r = 0 \tag{A2}$$

Yawing moment:

$$-N_\beta\beta - sN_p\phi + \left(s - N_r\right)r = 0 \tag{A3}$$

where $\beta = \frac{v}{V}$.

For nontrivial solutions, s must be a root of the characteristic equation

$$As^4 + Bs^3 + Cs^2 + Ds + E = 0 \tag{A4}$$

where

$$A = 1$$

$$B = -Y_v - L_p - N_r$$

$$C = N_\beta + L_pN_r - L_rN_p + Y_v\left(L_p + N_r\right) - L_\beta Y_p - N_\beta Y_r$$

$$D = L_\beta N_p - L_pN_\beta - Y_v\left(L_pN_r - L_rN_p\right) - \frac{g}{V}L_\beta - L_\beta\left(Y_rN_p - N_rY_p\right) + N_\beta\left(Y_rL_p - L_rY_p\right)$$

$$E = \frac{g}{V}\left(L_\beta N_r - L_rN_\beta\right)$$

The damping and period of a mode of motion, in seconds, are given by the equations $t_{1/2} = -\frac{0.693}{\sigma}$ and $P = \frac{2\pi}{\omega}$, respectively, where σ and ω are the real and imaginary parts of the roots of the stability equation. Additional stability characteristics may be obtained by the following relations:

$$\left.\begin{aligned} C_{1/2} &= \frac{t_{1/2}}{P} \\ \omega_n &= \sqrt{\sigma^2 + \omega^2} \\ \zeta &= -\frac{\sigma}{\omega_n} \end{aligned}\right\} \tag{A5}$$

The magnitude and phase relationships between ϕ, β, and ψ may be obtained by substituting the complex roots into the equations of motion and by solving the resulting equations for the appropriate magnitude and phase characteristics.

The general equations of motion are simplified for hovering flight. The stability derivatives N_p, N_β, and L_r are usually negligible, and the yawing-moment equation becomes uncoupled from the side-force and rolling-moment equations. The resulting characteristic equation for hovering flight with roll-attitude stabilization L_ϕ is:

$$\left(s - N_r\right)\left[s^3 - \left(Y_v + L_p\right)s^2 + \left(Y_v L_p - L_\phi\right)s + \left(Y_v L_\phi - L_v g\right)\right] = 0 \qquad \text{(A6)}$$

One root of the characteristic equation (equal to the value of N_r) is immediately known. The remaining cubic describes the oscillation involving the rolling and sideward degrees of freedom.

APPENDIX B

INSTRUMENTATION AND DATA REDUCTION

The present investigation utilized a six-channel return signal analyzer to obtain the dynamic oscillatory derivatives. This equipment permitted extremely rapid data acquisition. A block diagram of the data-reduction system is shown in figure 20.

The output of one strain-gage element, for example, the rolling moment, can be expressed as

$$e_l = M_X k_l E \tag{B1}$$

This voltage signal is returned to two of the signal analyzer channels. In one channel, the rolling-moment signal is multiplied by the in-phase voltage return signal of the sine-cosine potentiometer $\left(E_R \sin \omega t\right)$; whereas, in the second channel, the moment voltage is multiplied by the out-of-phase signal $\left(E_R \cos \omega t\right)$. The resulting voltages for the multiplications are

$$\text{In-phase voltage} = E_{in} = e_l E_R \sin \omega t \tag{B2}$$

$$\text{Out-of-phase voltage} = E_{out} = e_l E_R \cos \omega t \tag{B3}$$

The total aerodynamic rolling moment M_X during forced-oscillation tests in roll can be expressed as

$$M_X = M_{X,st} + M_{X_p} \Delta p + M_{X_{\dot{p}}} \Delta \dot{p} + M_{X_\beta} \Delta \beta + M_{X_{\dot{\beta}}} \Delta \dot{\beta} \tag{B4}$$

The oscillatory motions generated by the forced-oscillation apparatus and the wind-tunnel constraints (wind fixed in direction) produce the following kinematical relations:

$$\left.\begin{aligned} \Delta\phi &= \Delta\phi_{max} \sin \omega t \\ \Delta\dot{\phi} &= \Delta p = \omega \, \Delta\phi_{max} \cos \omega t \\ \Delta\ddot{\phi} &= \Delta\dot{p} = -\omega^2 \Delta\phi_{max} \sin \omega t \\ \Delta\beta &\approx \Delta\phi_{max} \sin \alpha \\ \Delta\dot{\beta} &\approx \Delta\dot{\phi}_{max} \sin \alpha \end{aligned}\right\} \tag{B5}$$

Substituting relations (B5), equation (B1), and equation (B4) into equations (B2) and (B3) yields (only the out-of-phase result is shown for a convenience)

$$E_{out} = E_R k_l E \cos \omega t \left[M_{X,st} + \left(M_{X_\beta} \sin \alpha - \omega^2 M_{X_{\dot{p}}} \right) \Delta\phi_{max} \sin \omega t \right.$$

$$\left. + \left(M_{X_p} + M_{X_{\dot{\beta}}} \sin \alpha \right) \omega \, \Delta\phi_{max} \cos \omega t \right] \tag{B6}$$

The out-of-phase analyzer channel finds the average value of this voltage as

$$\overline{E}_{out} = \frac{1}{T} \int_{t_o}^{t_o+T} E_{out} \, dt \tag{B7}$$

Substituting equation (B6) into equation (B7) and integrating yields

$$\overline{E}_{out} = \frac{K_l \omega \, \Delta\phi_{max}}{2} \left(M_{X_p} + M_{X_{\dot{\beta}}} \sin \alpha \right) \tag{B8}$$

for which

$$M_{X_p} + M_{X_{\dot{\beta}}} \sin \alpha = \frac{2\overline{E}_{out}}{K_l \omega \, \Delta\phi_{max}}$$

where

$$K_l = E_R k_l E$$

The in-phase derivative is obtained from the second analyzer channel as

$$M_{X_\beta} \sin \alpha - \omega^2 M_{X_{\dot{p}}} = \frac{2\overline{E}_{in}}{K_l \, \Delta\phi_{max}} \tag{B9}$$

Equations (B8) and (B9) can be nondimensionalized to obtain standard nondimensional derivative combinations:

$$C_{l_p} + C_{l_{\dot{\beta}}} \sin \alpha = \frac{2V}{q_\infty S b^2} \left(M_{X_p} + M_{X_{\dot{\beta}}} \sin \alpha \right)$$

$$C_{l_\beta} \sin \alpha - \left(\frac{\omega b}{2V} \right)^2 C_{l_{\dot{p}}} = \frac{1}{q_\infty S b} \left(M_{X_\beta} \sin \alpha - \omega^2 M_{X_{\dot{p}}} \right)$$

The present investigation was conducted with a value of angle of attack equal to zero; therefore, the out-of-phase derivative was entirely C_{l_p} and the in-phase derivative was due to $C_{l_{\dot{p}}}$.

REFERENCES

1. Newsom, William A., Jr.; and Kirby, Robert H.: Flight Investigation of Stability and Control Characteristics of a 1/9-Scale Model of a Four-Propeller Tilt-Wing V/STOL Transport. NASA TN D-2443, 1964.

2. Goodson, Kenneth W.: Longitudinal Aerodynamic Characteristics of a Flapped Tilt-Wing Four-Propeller V/STOL Transport Model. NASA TN D-3217, 1966.

3. Goodson, Kenneth W.: Effect of Ground Proximity on the Longitudinal, Lateral, and Control Aerodynamic Characteristics of a Tilt-Wing Four-Propeller V/STOL Model. NASA TN D-4237, 1967.

4. Chambers, Joseph R.; and Grafton, Sue B.: Static and Dynamic Longitudinal Stability Derivatives of a Powered 1/9-Scale Model of a Tilt-Wing V/STOL Transport. NASA TN D-3591, 1966.

5. Chambers, Joseph R.; and Grafton, Sue B.: Calculation of the Dynamic Longitudinal Stability of a Tilt-Wing V/STOL Aircraft and Correlation With Model Flight Tests. NASA TN D-4344, 1968.

6. Chambers, Joseph R.; and Boisseau, Peter C.: A Theoretical Analysis of the Dynamic Lateral Stability and Control of a Parawing Vehicle. NASA TN D-3461, 1966.

7. Anon.: Helicopter Flying and Ground Handling Qualities; General Requirements for Mil. Specif. MIL-H-8501A, Sept. 7, 1961.

8. Anon.: Flying Qualities of Piloted Airplanes. Mil. Specif. MIL-F-8785(ASG), Sept. 1, 1954; Amendment-4, Apr. 17, 1959.

9. Anon.: Recommendations for V/STOL Handling Qualities. AGARD Rep. 408A, Oct. 1964.

TABLE I.- MASS AND GEOMETRIC CHARACTERISTICS OF THE V/STOL TRANSPORT

Gross weight, lb (N)	37 439 (166 529)
Moment of inertia in roll, slug-ft^2 (kg-m^2)	173 000 (234 553)
Moment of inertia in yaw, slug-ft^2 (kg-m^2)	267 000 (361 999)
Wing loading, lb/ft^2 (N/m^2)	70.0 (3 352)
Fuselage:	
Length, ft (m)	50.0 (15.2)
Cross-sectional area, maximum, ft^2 (m^2)	81.8 (7.6)
Height, ft (m)	12.2 (3.7)
Width, ft (m)	9.1 (2.8)
Wing:	
Area, ft^2 (m^2)	534.4 (49.6)
Span, ft (m)	67.5 (20.6)
Aspect ratio	8.53
Mean aerodynamic chord, ft (m)	8.07 (2.5)
Airfoil section	NACA 63_3-318
Tip chord, ft (m)	6.0 (1.8)
Root chord, ft (m)	9.8 (2.9)
Taper ratio	0.61
Sweepback of quarter chord, deg	4.13
Dihedral angle, deg	-2.12
Pivot location, percent root chord	42.5
Aileron, each:	
Chord, percent wing chord	25
Area, ft^2 (m^2)	31.1 (2.9)
Flap, each:	
Type	Double slotted
Chord, percent wing chord	47
Span	Full
Slat, each:	
Inboard, 0.45 wing semispan to 0.69 wing semispan	Chord, 0.2 wing chord inboard to 0.10 wing chord outboard
Outboard, 0.85 wing semispan to 1.00 wing semispan	Chord, 0.1 wing chord full length

TABLE I.- MASS AND GEOMETRIC CHARACTERISTICS OF THE V/STOL TRANSPORT – Concluded

Vertical tail:	
Area, ft^2 (m^2)	130.0 (12.1)
Span, ft (m)	15.6 (4.8)
Aspect ratio	1.87
Airfoil section:	
Root	NACA 0018
Tip	NACA 0012
Tip chord, ft (m)	3.3 (1.0)
Root chord, ft (m)	13.3 (4.1)
Taper ratio	0.25
Sweepback of quarter chord, deg	26
Rudder:	
Tip chord, ft (m)	1.1 (0.3)
Root chord, ft (m)	3.8 (1.1)
Tail length, center of gravity to 0.25 mean aerodynamic chord, ft (m)	21.4 (6.5)
Horizontal tail:	
Area, ft^2 (m^2)	170.9 (15.9)
Aspect ratio	5.68
Airfoil section:	
Root	NACA 0015
Tip	NACA 0012
Tip chord, ft (m)	3.5 (1.1)
Root chord, ft (m)	7.0 (2.1)
Span, ft (m)	31.14 (9.5)
Taper ratio	0.50
Sweepback of quarter chord, deg	9.50
Mean aerodynamic chord, ft (m)	5.5 (1.7)
Tail length, center of gravity to 0.25 mean aerodynamic chord, ft (m)	24.8 (7.6)
Propellers:	
Main:	
Number of blades	4
Diameter, ft (m)	15.5 (4.7)
Tail:	
Number of blades	3
Diameter, ft (m)	8.0 (2.4)
Moment arm, wing pivot to rotor center, ft (m)	32.0 (9.8)

TABLE II.- DIMENSIONAL STABILITY DERIVATIVES FOR FULL-SCALE AIRCRAFT

(a) U.S. Customary Units

i_w, deg	V, ft/sec	Y_v, per sec	Y_p, ft/sec	Y_r, ft/sec	L_v, per ft-sec	L_p, per sec	L_r, per sec	N_v, per ft-sec	N_p, per sec	N_r, per sec
0	277.6	-0.262	2.998	2.054	-0.0087	-1.705	0.440	0.0024	0.069	-1.106
10	128.9	-.126	-.954	1.173	-.0059	-1.096	.457	.0022	-.173	-.594
20	104.6	-.111	-1.485	1.297	-.0064	-.914	.469	.0021	-.175	-.531
30	81.9	-.108	-1.882	1.507	-.0069	-.604	.430	.0028	-.195	-.483
40	67.4	-.109	-2.319	.371	-.0085	-.441	.415	.0069	-.201	-.449
50	58.2	-.127	-2.578	-.105	-.0099	-.348	.382	.0083	-.196	-.426
60	47.3	-.128	-2.720	-.284	-.0092	-.335	.327	.0073	-.094	-.409
70	35.8	-.120	-2.051	-.265	-.0085	-.256	.211	.0005	.024	-.381
90	0	-.108	-3.742	0	-.0082	-.124	0	0	0	-.338

(b) SI Units

i_w, deg	V, m/sec	Y_v, per sec	Y_p, m/sec	Y_r, m/sec	L_v, per m-sec	L_p, per sec	L_r, per sec	N_v, per m-sec	N_p, per sec	N_r, per sec
0	84.6	-0.262	0.9138	0.6261	-0.0027	-1.705	0.440	0.00073	0.069	-1.106
10	39.3	-.126	-.2908	.3575	-.0018	-1.096	.457	.00067	-.173	-.594
20	31.9	-.111	-.4526	.3953	-.0019	-.914	.469	.00064	-.175	-.531
30	25.0	-.108	-.5736	.4593	-.0021	-.604	.430	.00085	-.195	-.483
40	20.5	-.109	-.7068	.1131	-.0026	-.441	.415	.00210	-.201	-.449
50	17.7	-.127	-.7858	-.0320	-.0030	-.348	.382	.00253	-.196	-.420
60	14.4	-.128	-.8291	-.0866	-.0028	-.335	.327	.00222	-.094	-.409
70	10.9	-.120	-.6251	-.0808	-.0026	-.256	.211	.00015	.024	-.381
90	0	-.108	-1.1406	0	-.0025	-.124	0	0	0	-.338

TABLE III.- SUMMARY OF CALCULATED STABILITY CHARACTERISTICS

i_w, deg	Mode	σ, per sec	ω, rad/sec	$t_{1/2}$, sec (a)	P, sec	$C_{1/2}$ (a)	ω_n, rad/sec	ζ (a)	$\left\|\frac{\phi}{\beta}\right\|$	$\left\|\frac{\phi}{\psi}\right\|$
0	Oscillatory	-0.569	±0.582	1.22	10.79	0.113	0.814	0.699	2.13	2.45
	Aperiodic	-.247	0	2.80						
	Aperiodic	-1.689	0	.41						
10	Oscillatory	-0.211	±0.649	3.29	9.68	0.339	0.682	0.309	0.91	1.20
	Aperiodic	-.135	0	5.14						
	Aperiodic	-1.259	0	.55						
20	Oscillatory	-0.132	±0.627	5.24	10.02	0.523	0.641	0.206	0.93	1.38
	Aperiodic	-.165	0	4.20						
	Aperiodic	-1.126	0	.62						
30	Oscillatory	-0.050	±0.665	13.92	9.45	1.474	0.667	0.075	0.89	1.42
	Aperiodic	-.164	0	4.23						
	Aperiodic	-.931	0	.74						
40	Oscillatory	-0.050	±0.827	13.87	7.60	1.826	0.829	0.060	0.72	0.98
	Aperiodic	-.053	0	13.05						
	Aperiodic	-.846	0	.92						
50	Oscillatory	-0.012	±0.842	55.91	7.46	7.496	0.843	0.015	0.72	0.99
	Aperiodic	-.057	0	12.10						
	Aperiodic	-.819	0	.85						
60	Oscillatory	0.014	±0.724	-50.48	8.68	-5.817	0.724	-0.019	0.68	1.08
	Aperiodic	-.105	0	6.58						
	Aperiodic	-.793	0	.87						
70	Oscillatory	0.201	±0.547	-3.45	11.49	-0.300	0.583	-0.345	0.73	25.28
	Aperiodic	-.380	0	1.83						
	Aperiodic	-.780	0	.89						
[b]90	Oscillatory	0.244	±0.553	-2.74	11.36	-0.250	0.605	-0.404	---	∞
	Aperiodic	-.338	0	2.05						
	Aperiodic	-.721	0	.59						

[a]Negative signs indicate unstable modes of motion. For example, if $t_{1/2} = -50.48$, then $t_2 = 50.48$ or if $C_{1/2} = -5.817$, then $C_2 = 5.817$.

[b]For hovering flight, $\left|\frac{\phi}{v_e}\right| = 1.17 \frac{\text{deg}}{\text{ft/sec}} \left(3.84 \frac{\text{deg}}{\text{m/sec}}\right)$.

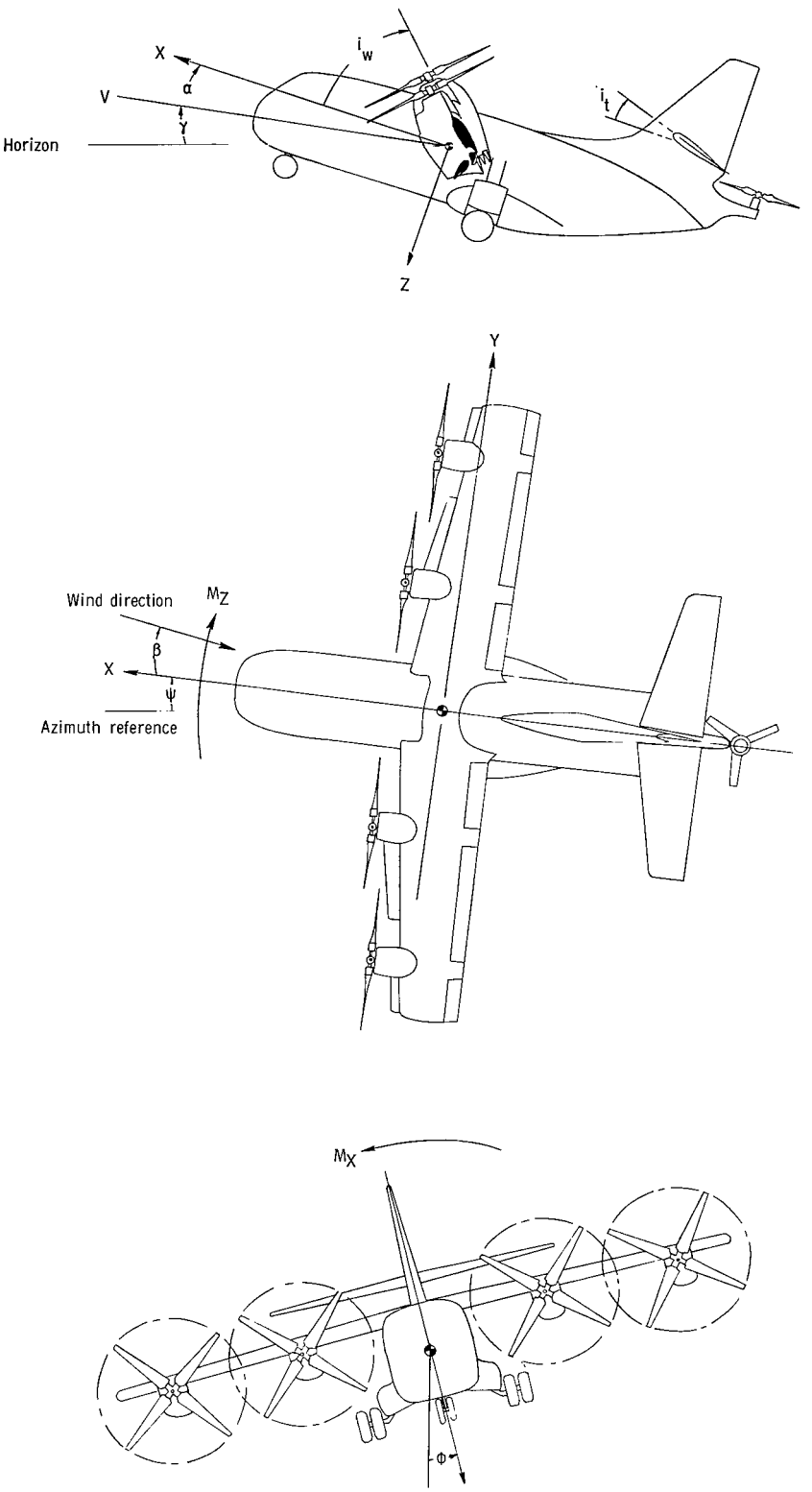

Figure 1.- System of body axes. Arrows indicate positive senses of moments and forces.

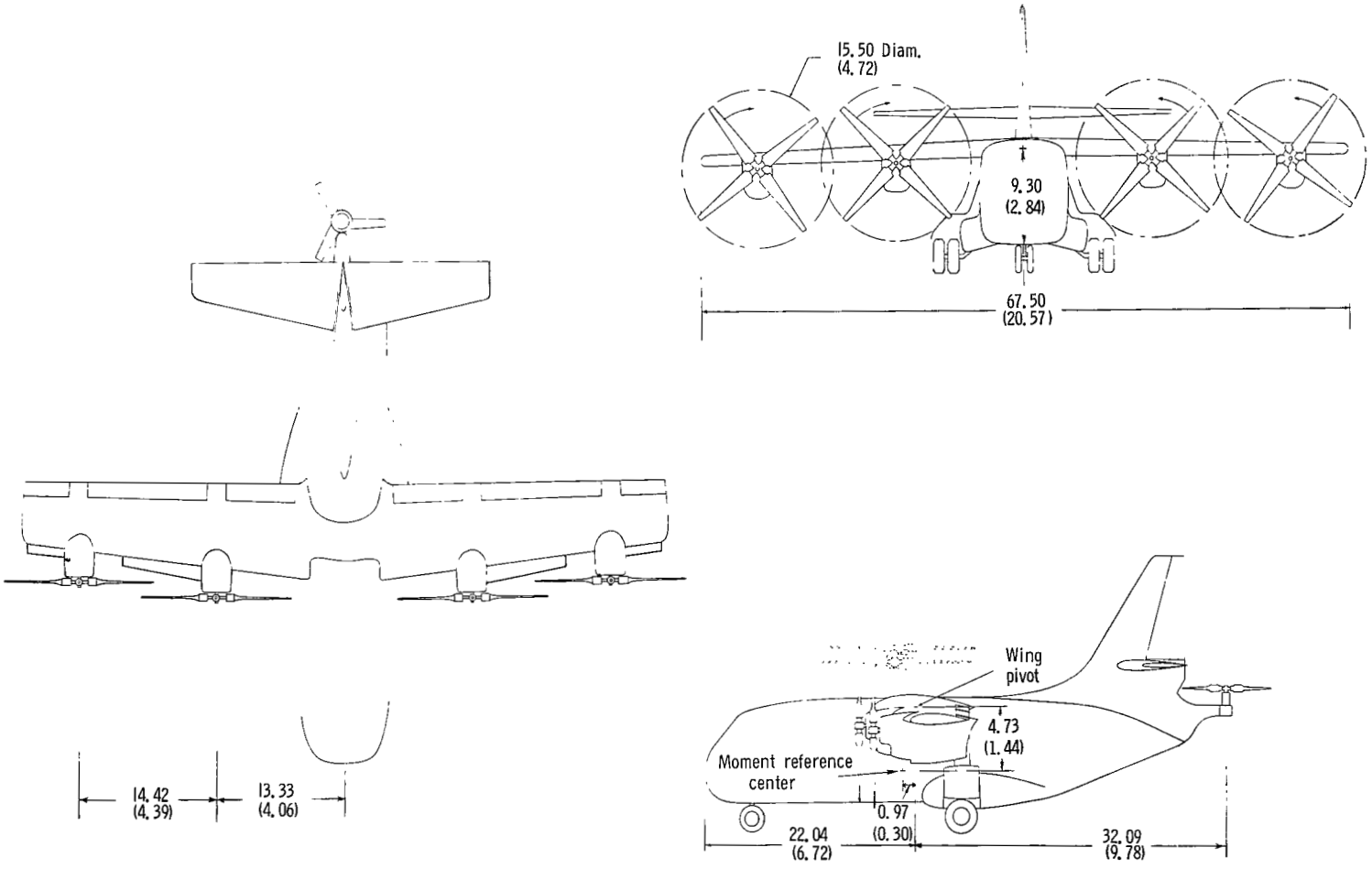

Figure 2.- Three-view drawing of the tilt-wing V/STOL transport. Dimensions are given in feet and parenthetically in meters.

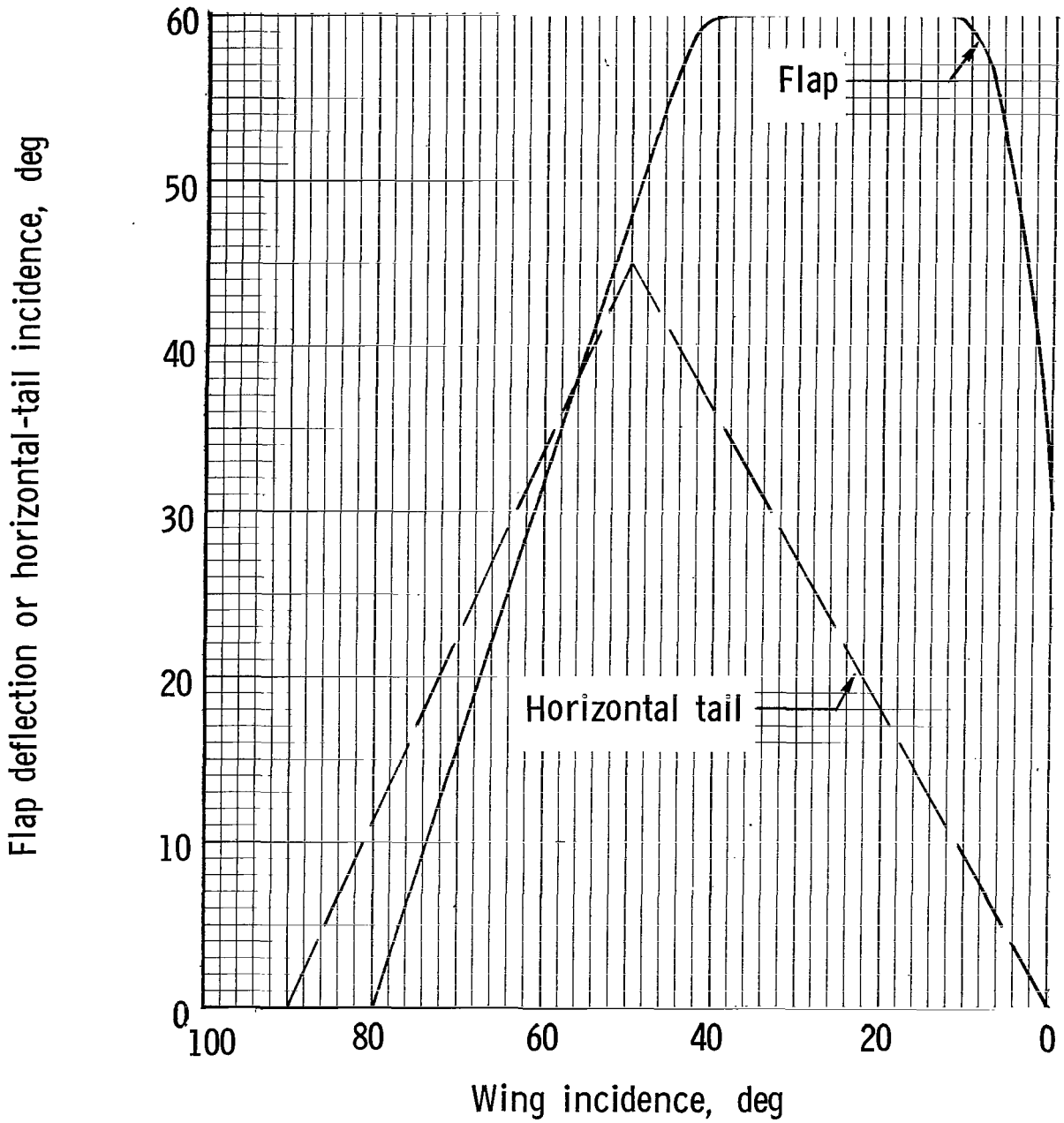

Figure 3.- Variation of flap deflection and horizontal-tail incidence with wing-incidence angle.

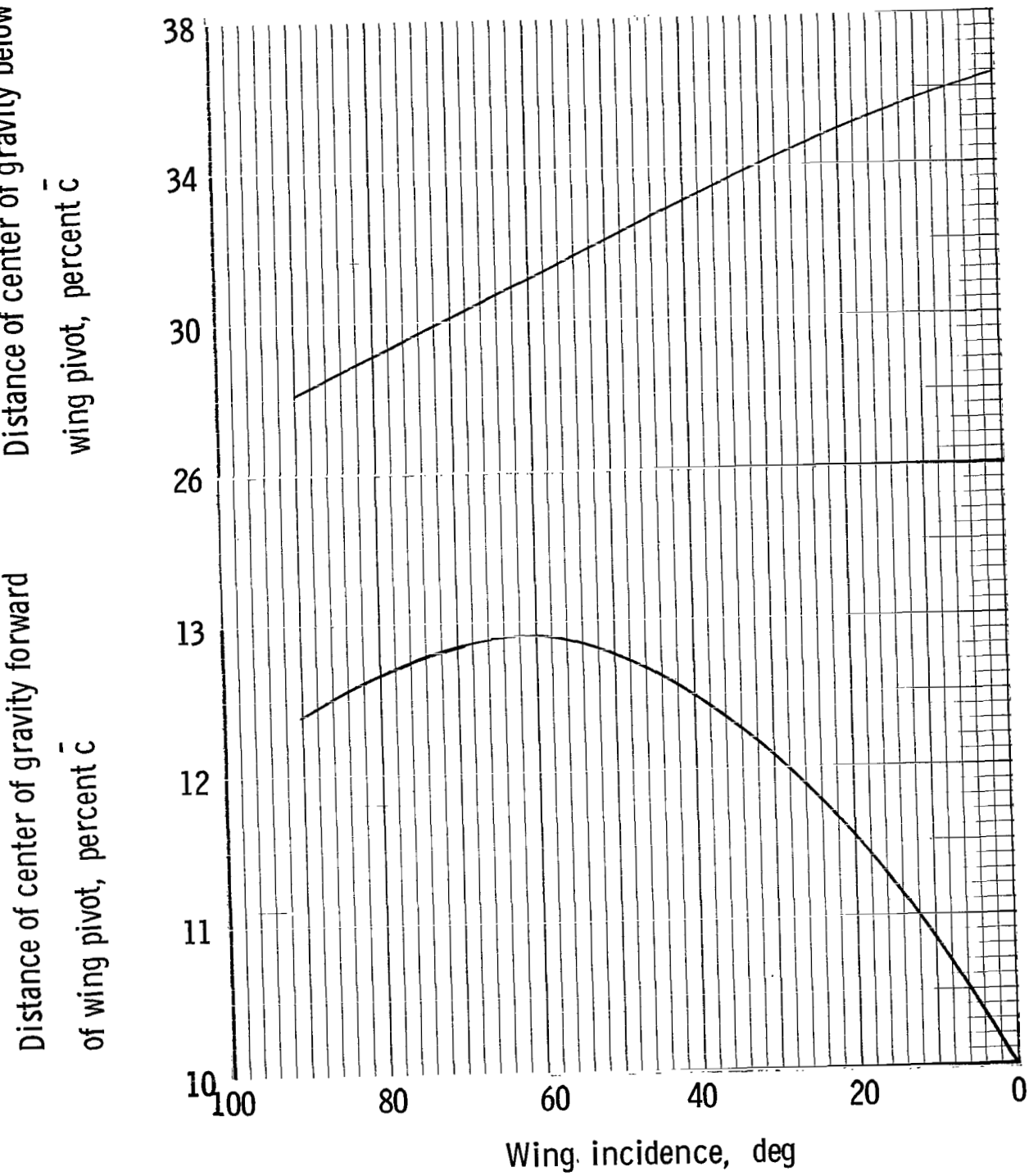

Figure 4.- Variation of airplane center-of-gravity location with wing-incidence angle.

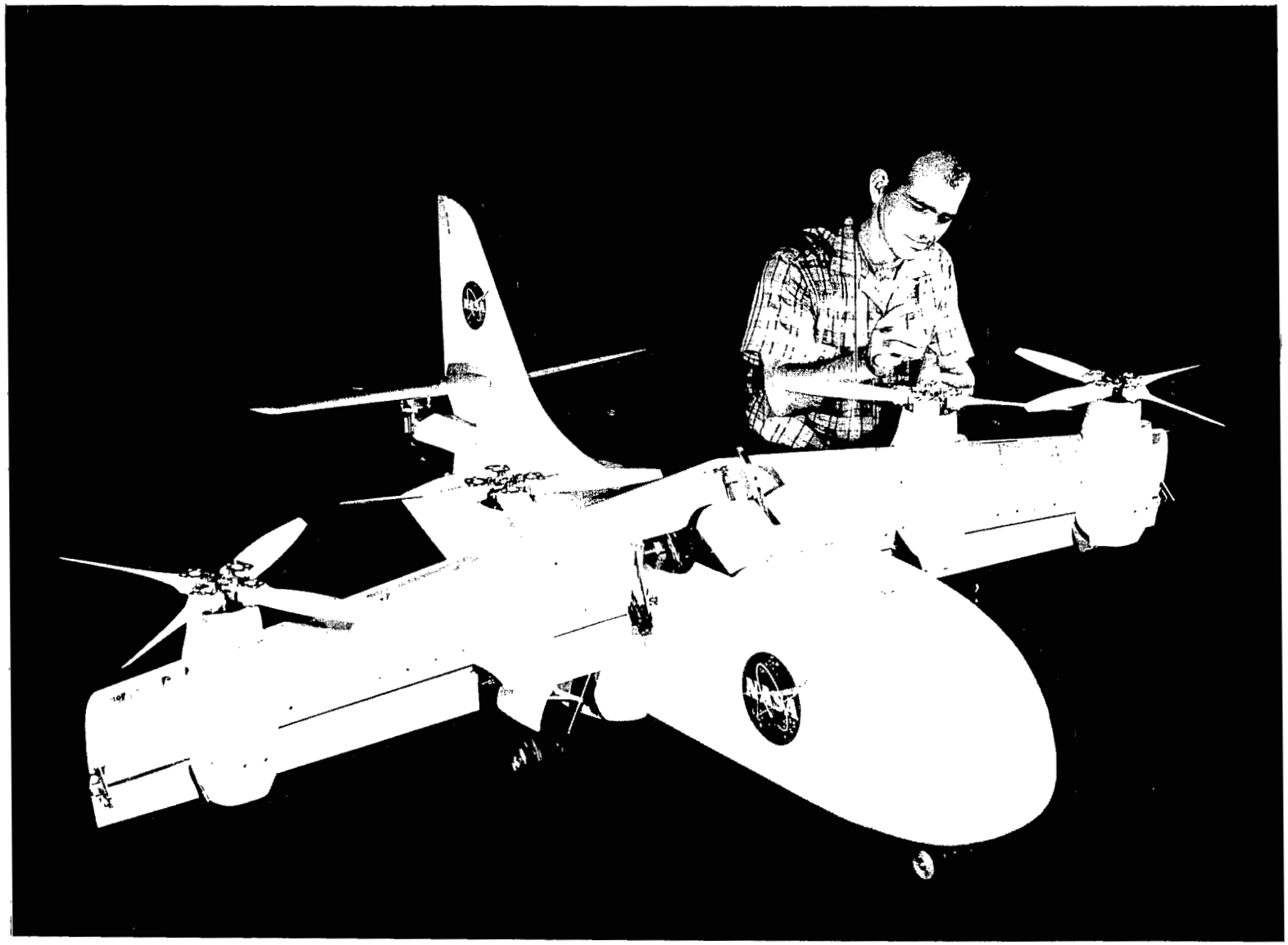

Figure 5.- Photograph of the 1/9-scale tilt-wing transport model. L-62-6318

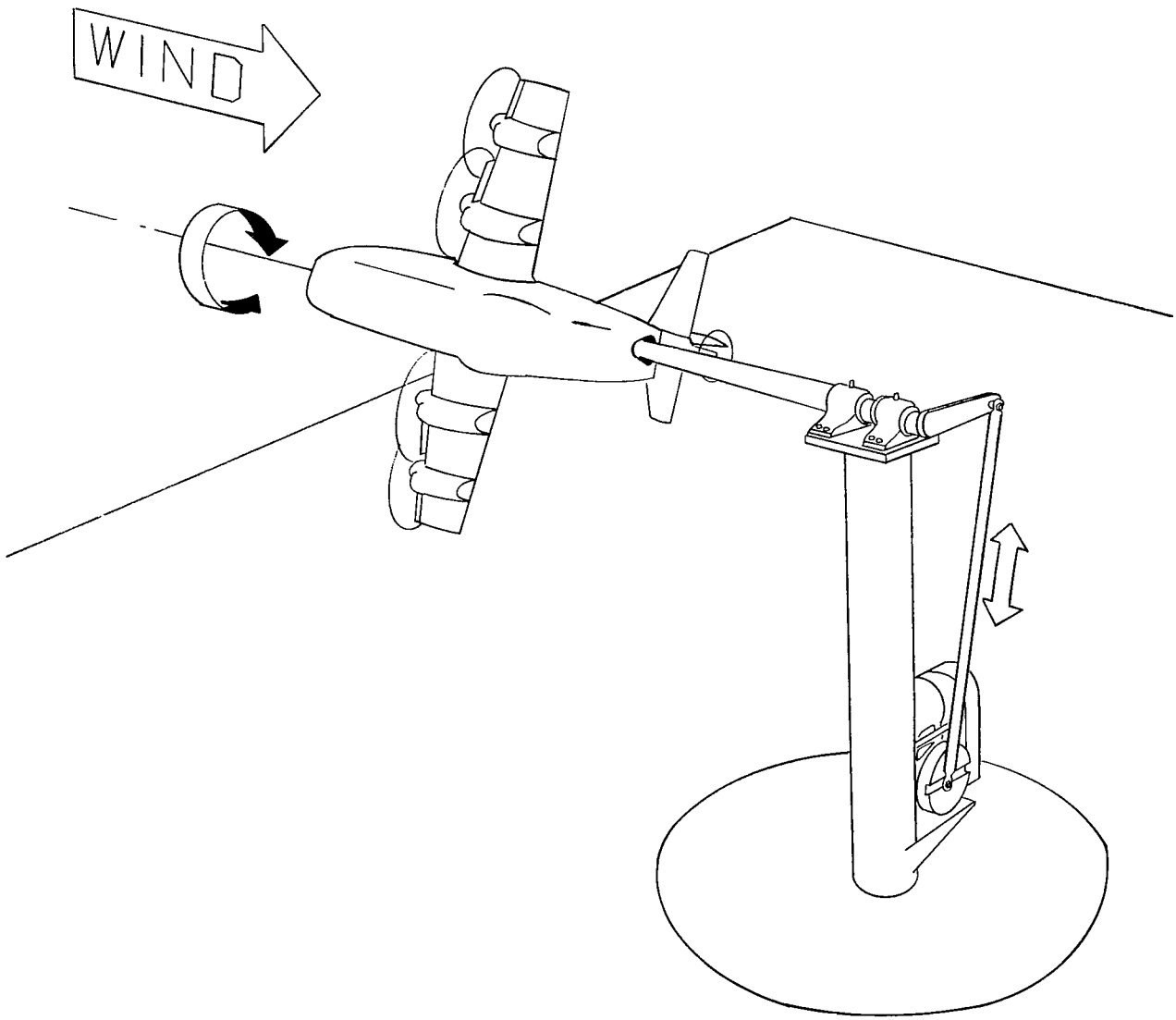

(a) Roll.

Figure 6.- Test setup for the forced-oscillation tests.

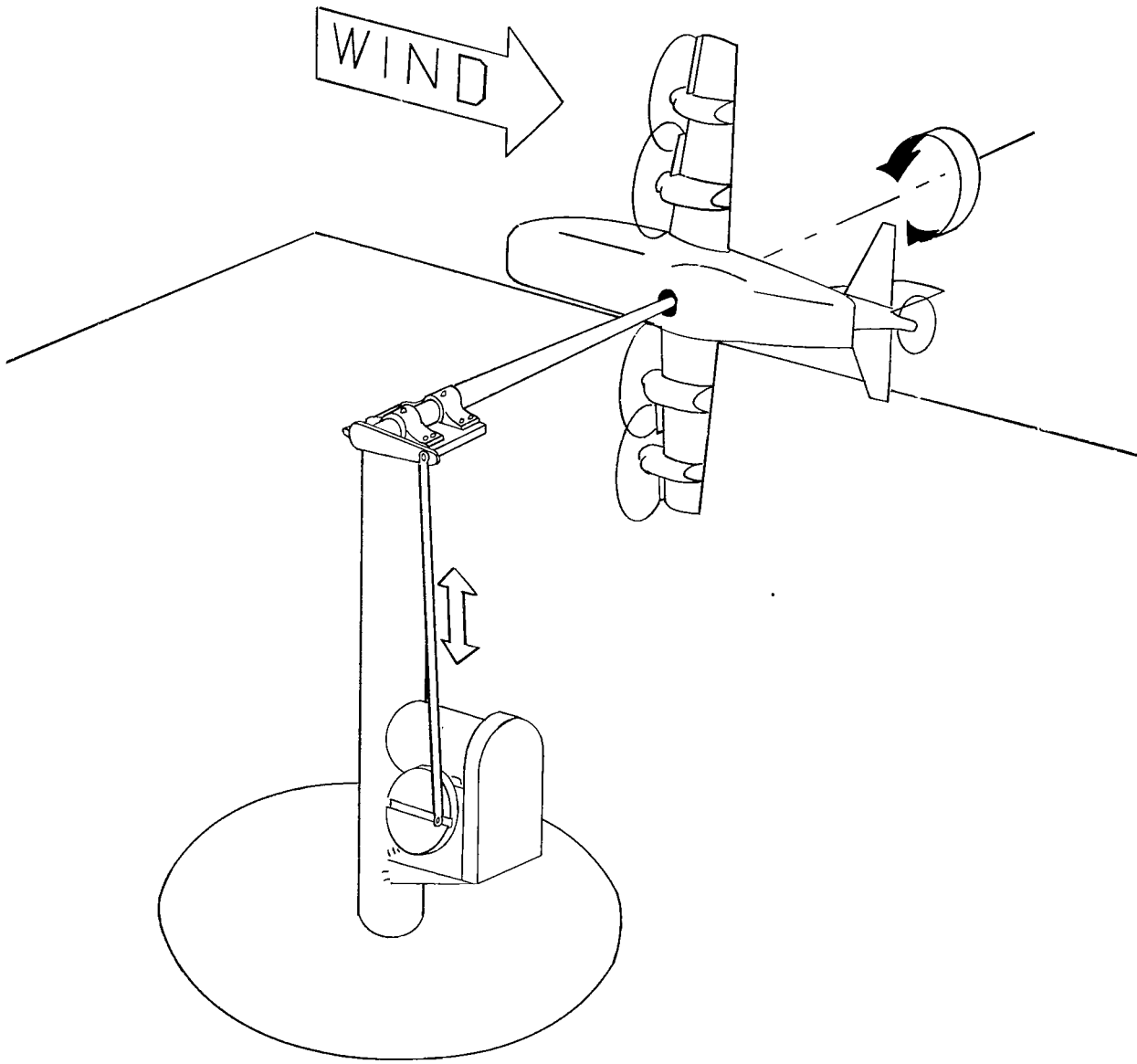

(b) Yaw.

Figure 6.- Concluded.

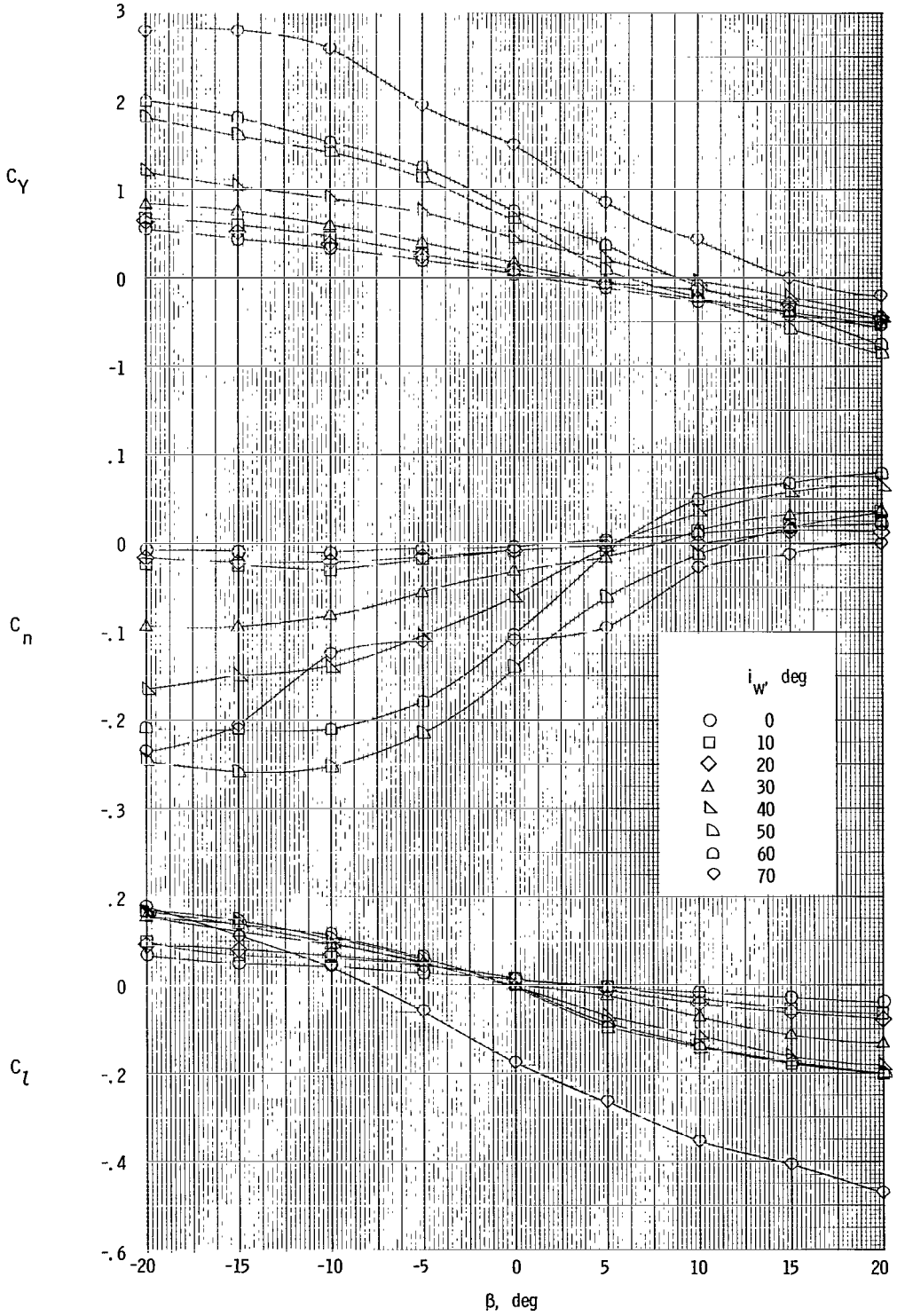

Figure 7.- Variation of static lateral-directional coefficients with sideslip angle. $\alpha = 0^o$.

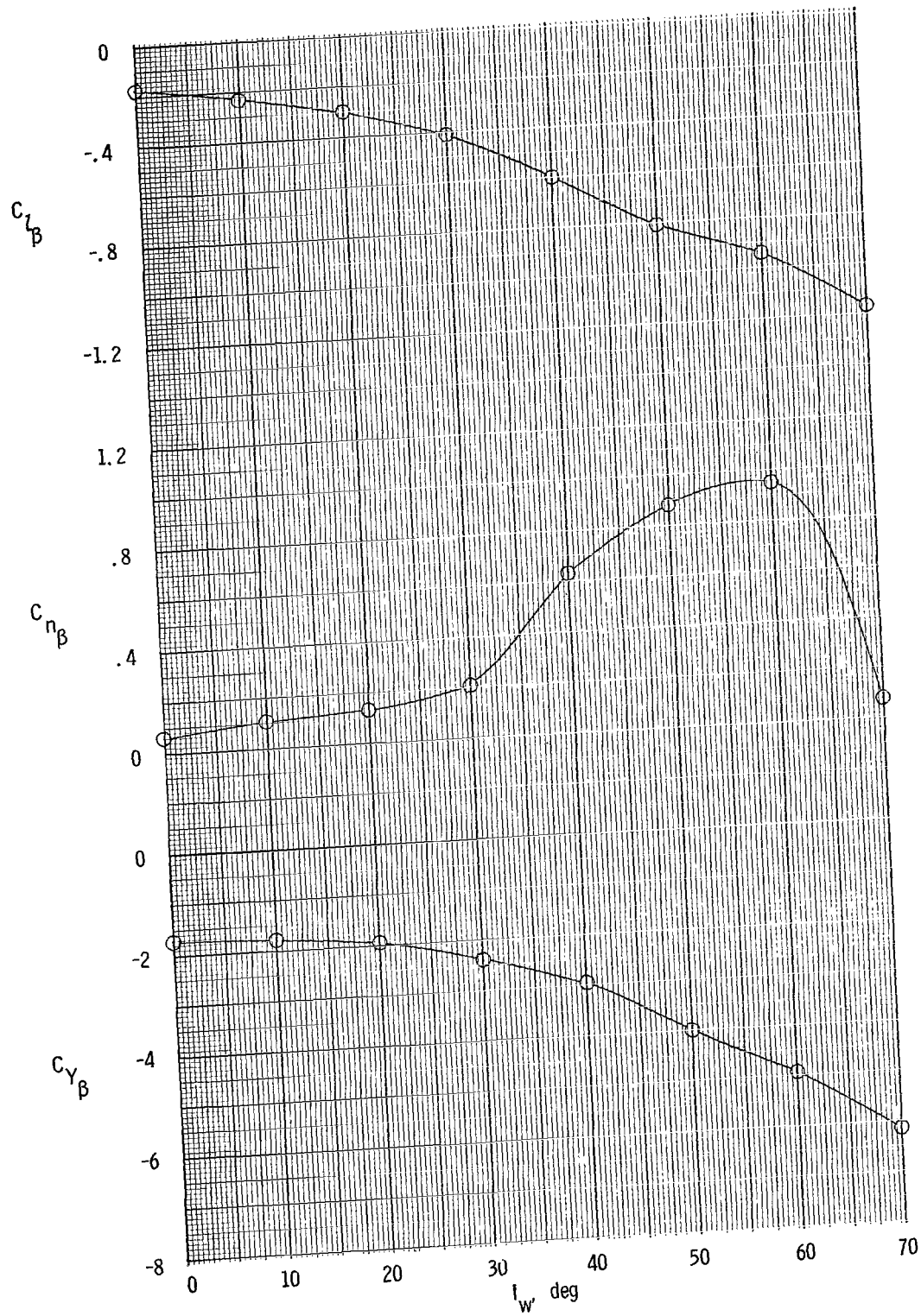

Figure 8.- Variation of static stability derivatives with wing-incidence angle. $\alpha = 0^o$.

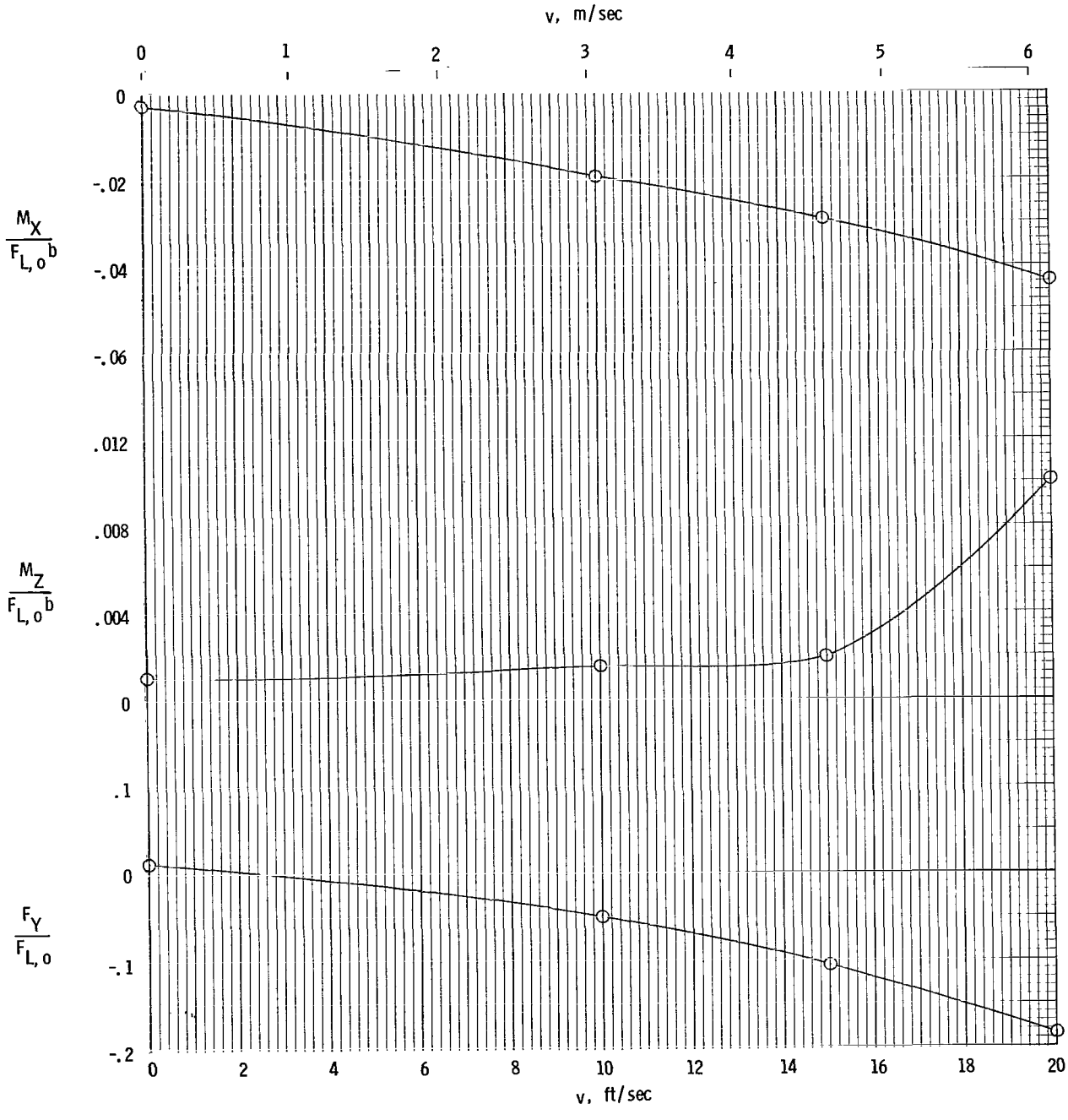

Figure 9.- Variation of lateral-directional forces and moments with lateral velocity for hovering configuration. $i_W = 90^0$; $F_{L,o} = 50.9$ lb (226.41 N); $\alpha = 0^0$.

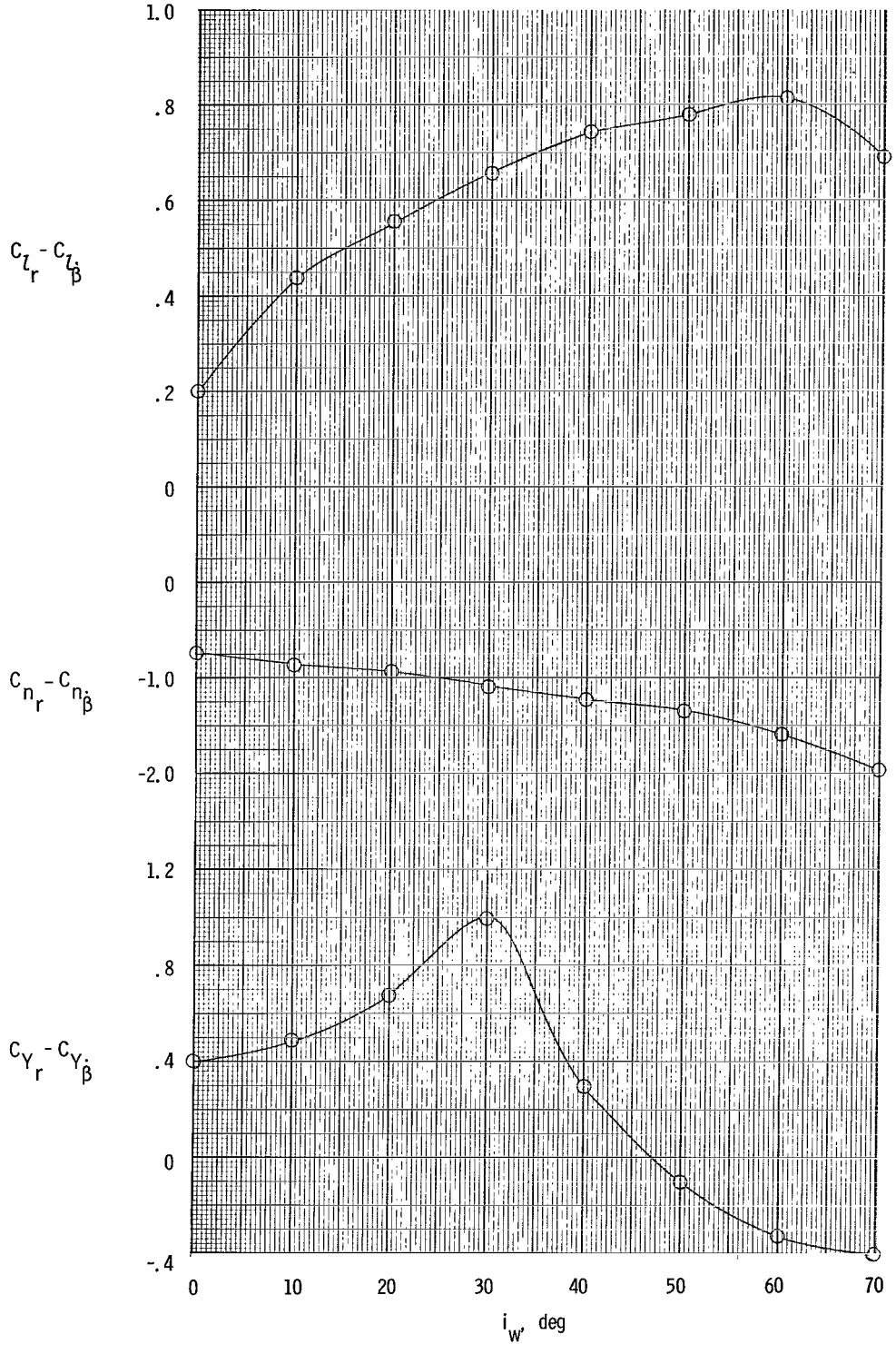

(a) Forced-oscillation test in yaw.

Figure 10.- Variation of dynamic derivatives with wing-incidence angle. $\alpha = 0^{\circ}$.

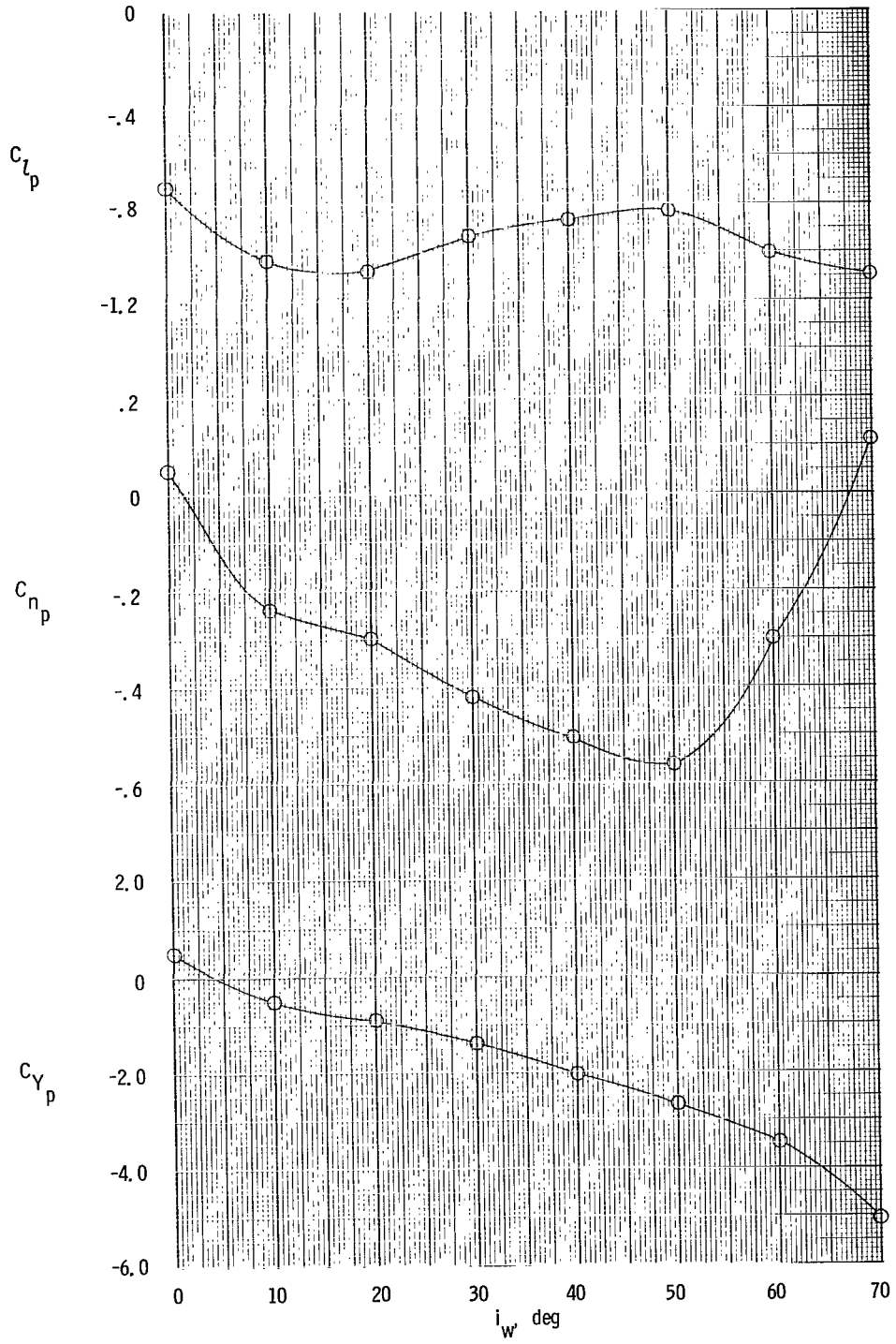

(b) Forced-oscillation test in roll.

Figure 10.- Concluded.

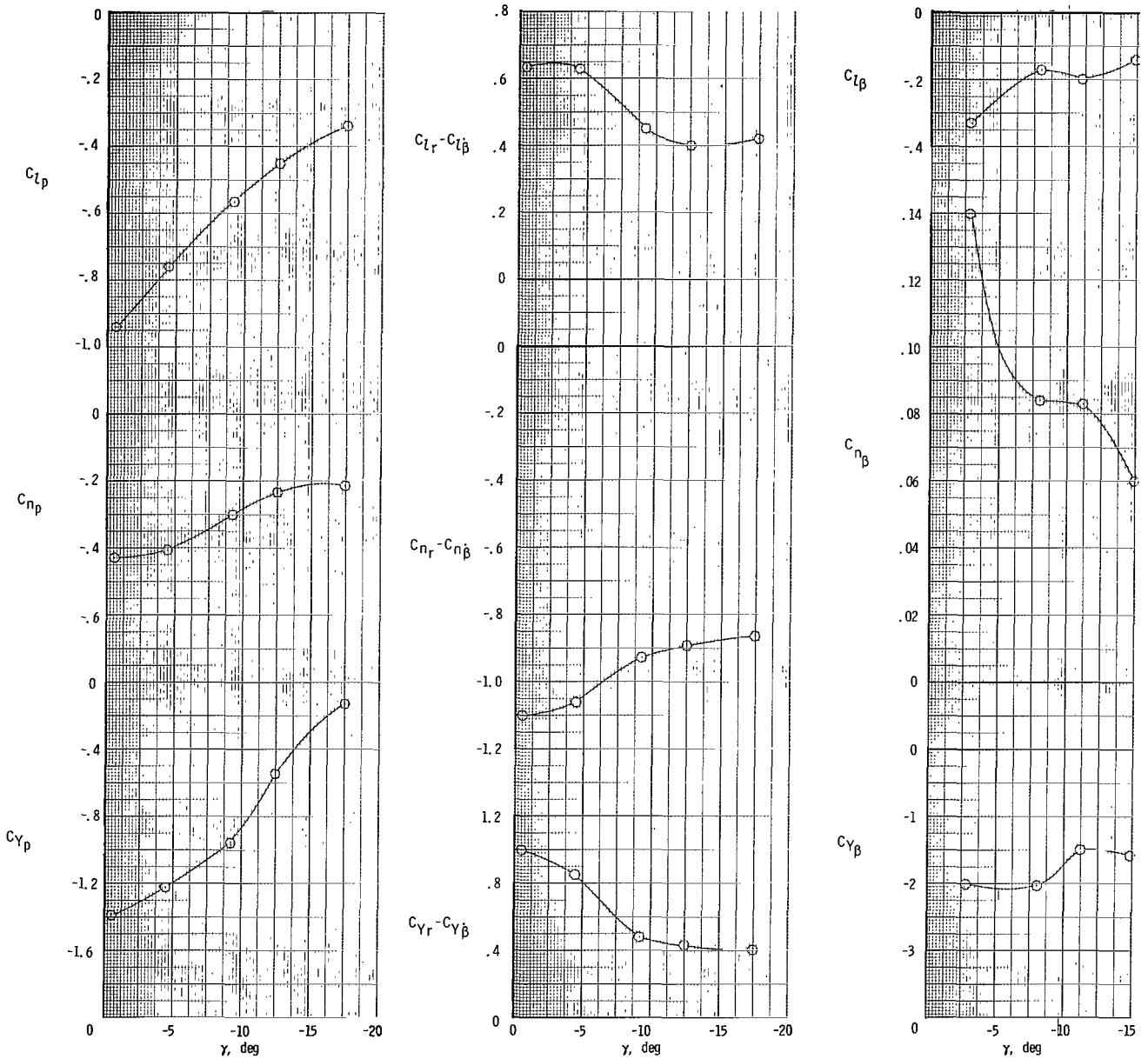

(a) Rolling. (b) Yawing. (c) Sideslip.

Figure 11.- Effect of power condition on lateral-directional derivatives. $i_W = 30^o$; $\alpha = 0^o$.

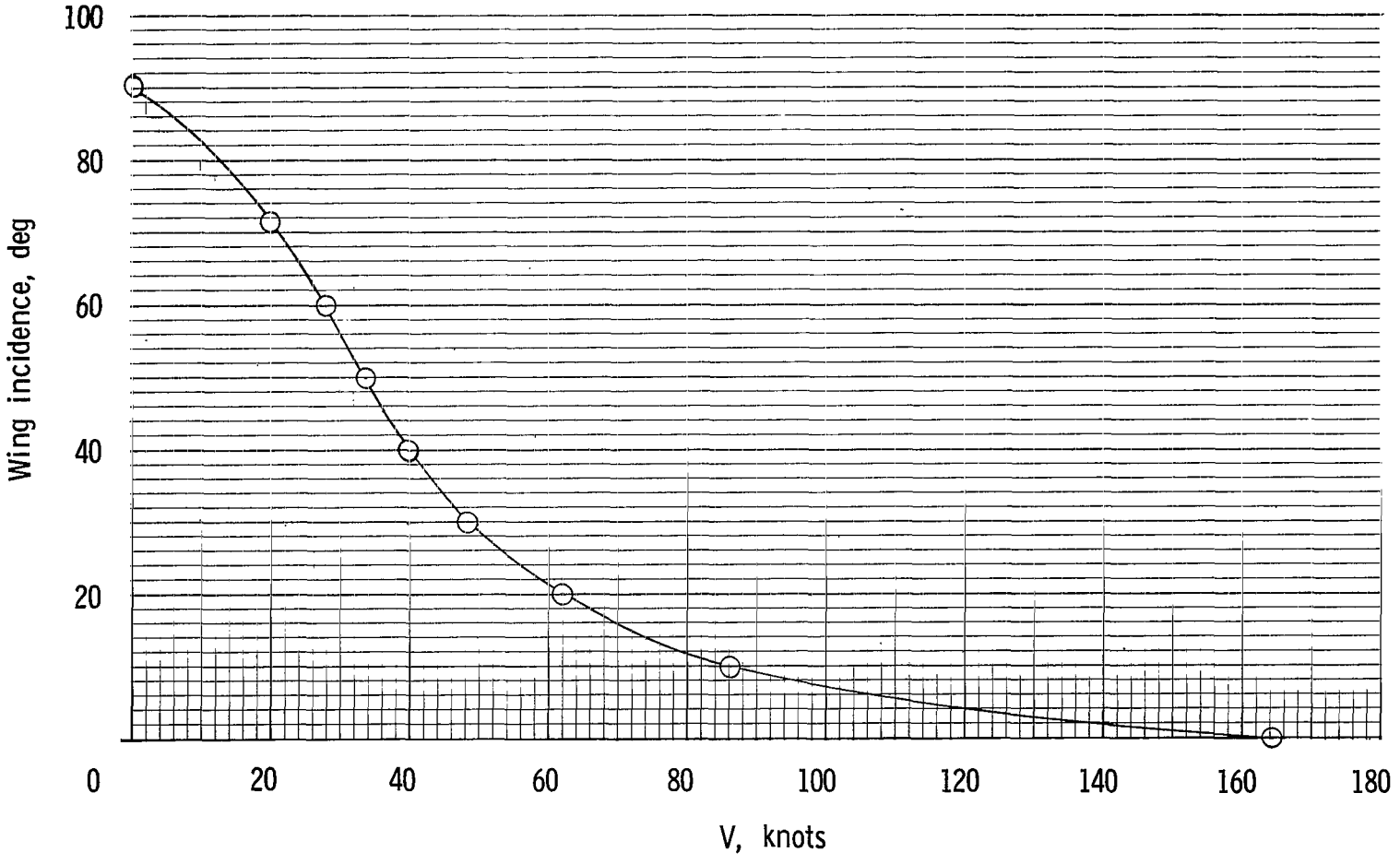

Figure 12.- Variation of trim velocity with wing-incidence angle. W/S = 70 lb/ft^2 (3350 N/m^2).

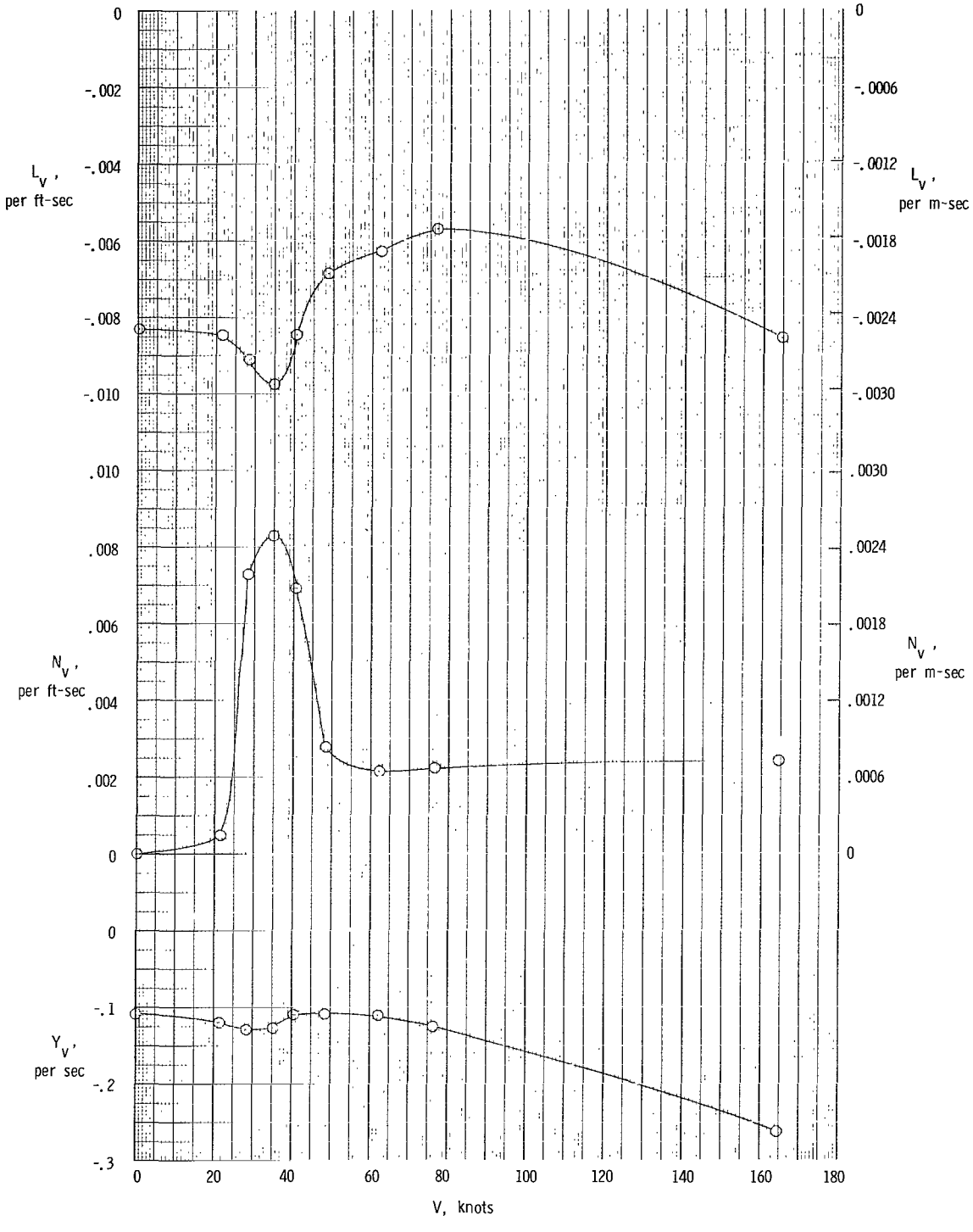

(a) Sideslip.

Figure 13.- Variation of dimensional stability derivatives of full-scale airplane with velocity. $\alpha = 0^{o}$.

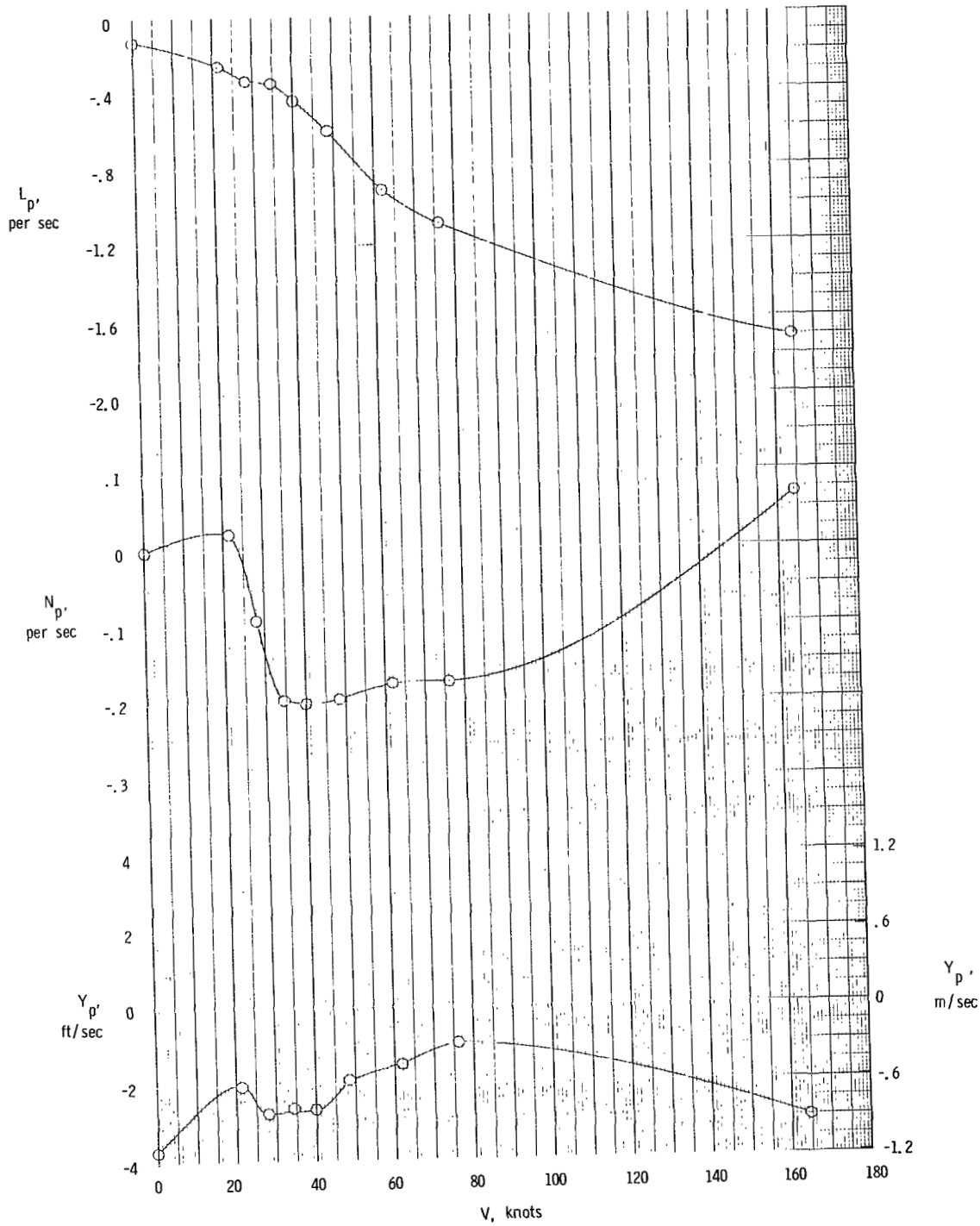

(b) Roll.

Figure 13.- Continued.

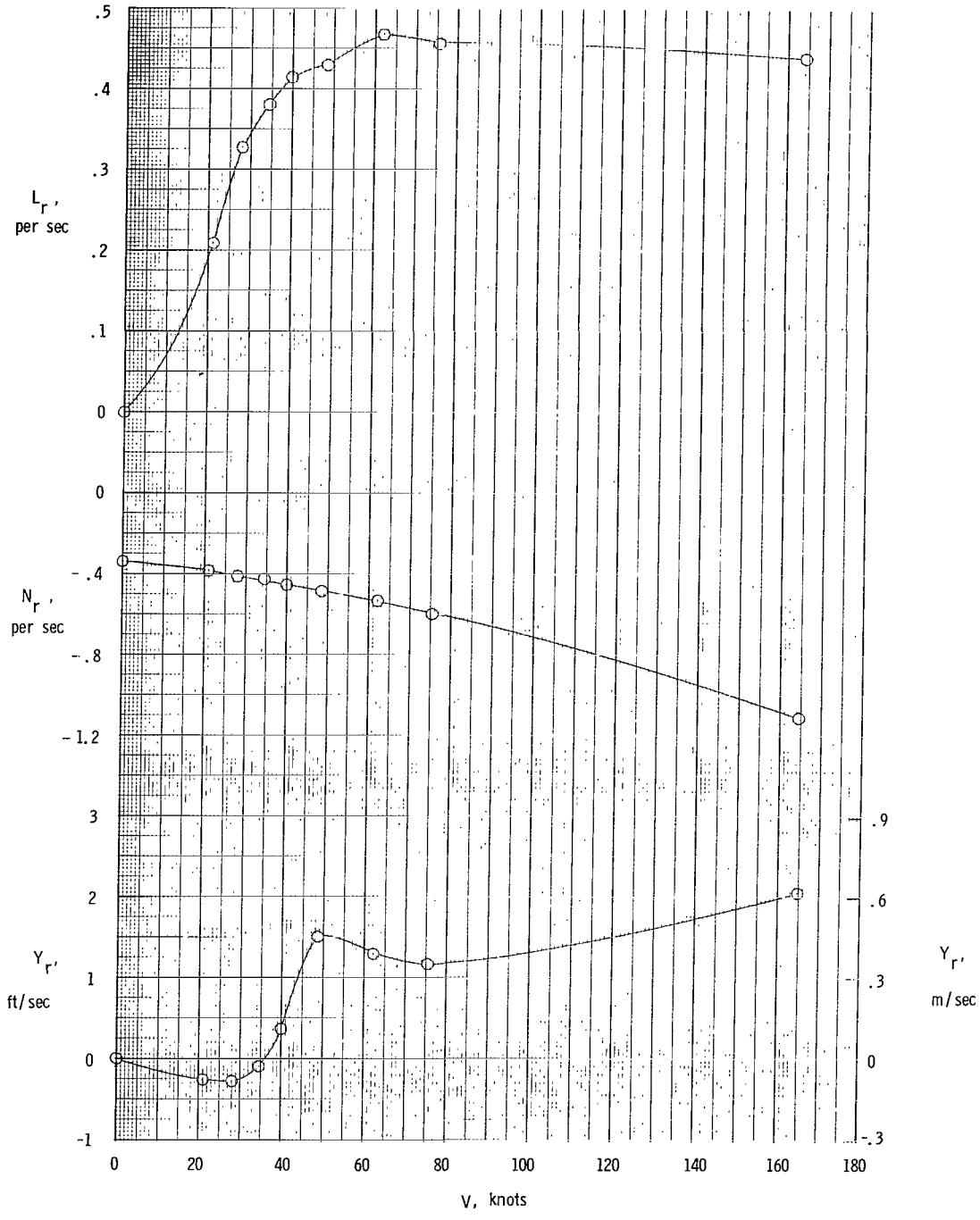

(c) Yaw.

Figure 13.- Concluded.

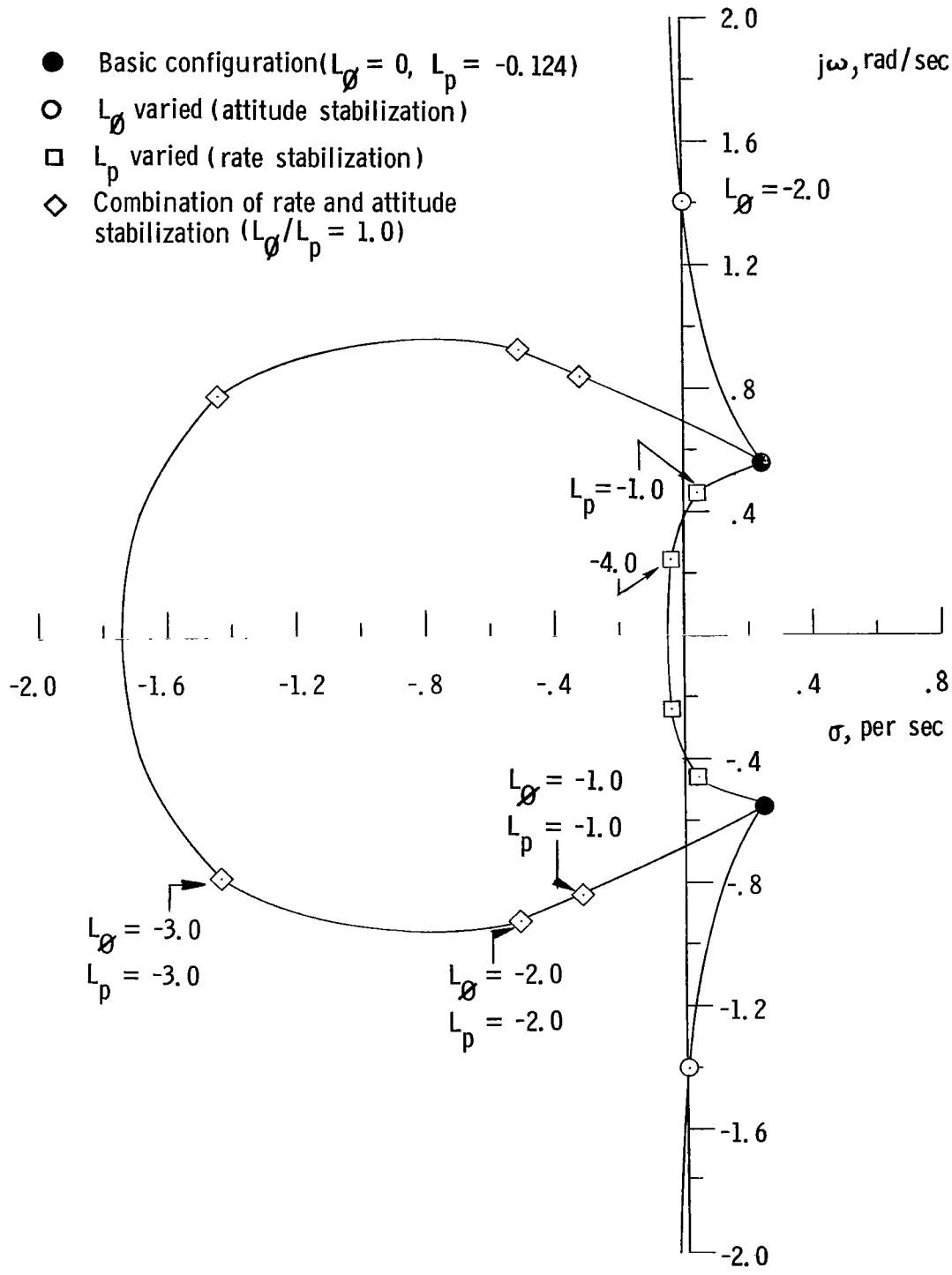

Figure 14.- Effect of roll-rate and roll-attitude stabilization for a full-scale airplane in hovering flight. (Unit for L_Φ is per sec^2 and unit for L_p and L_Φ/L_p is per sec.)

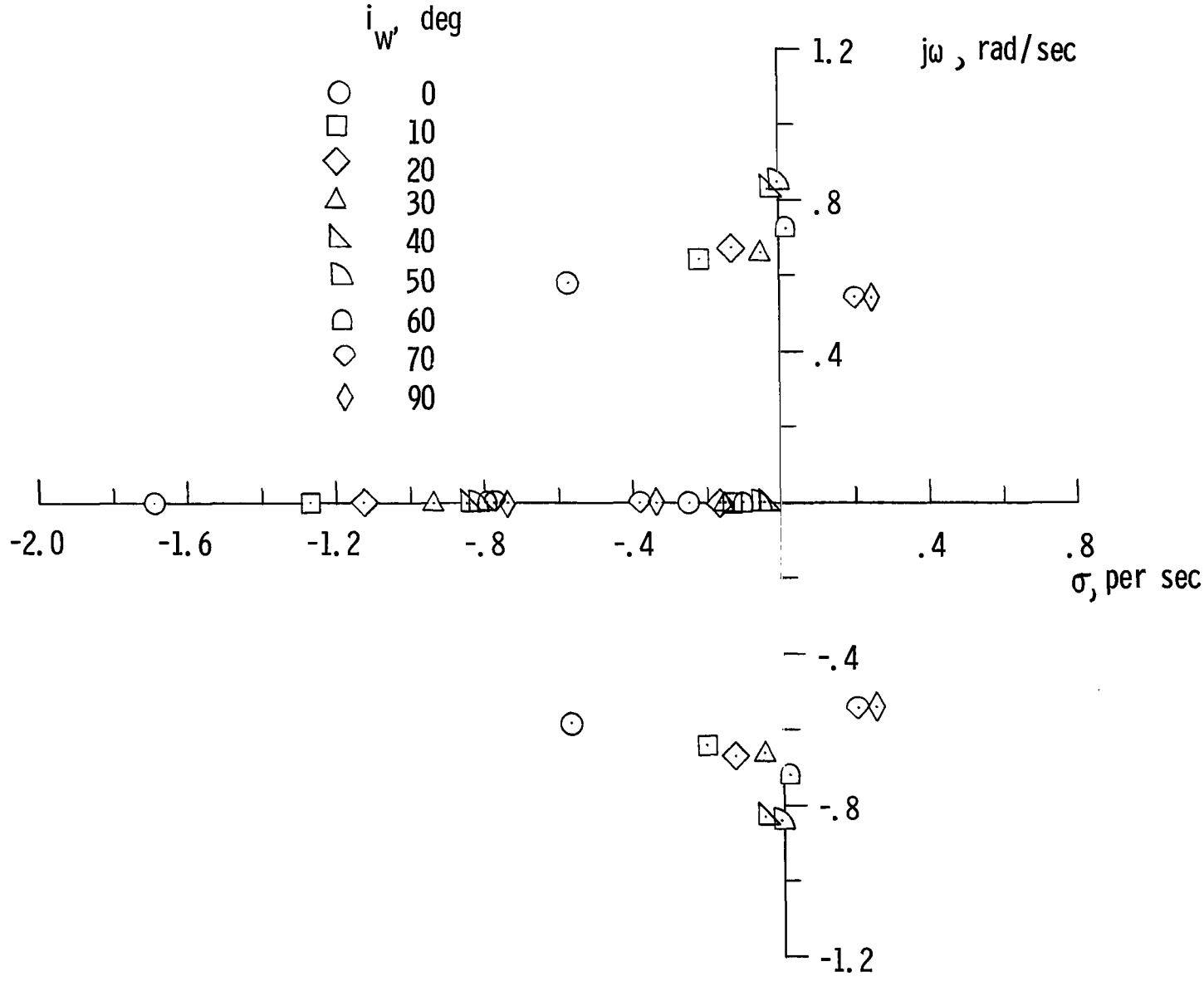

Figure 15.- Effect of wing incidence on the root locations on the complex plane.

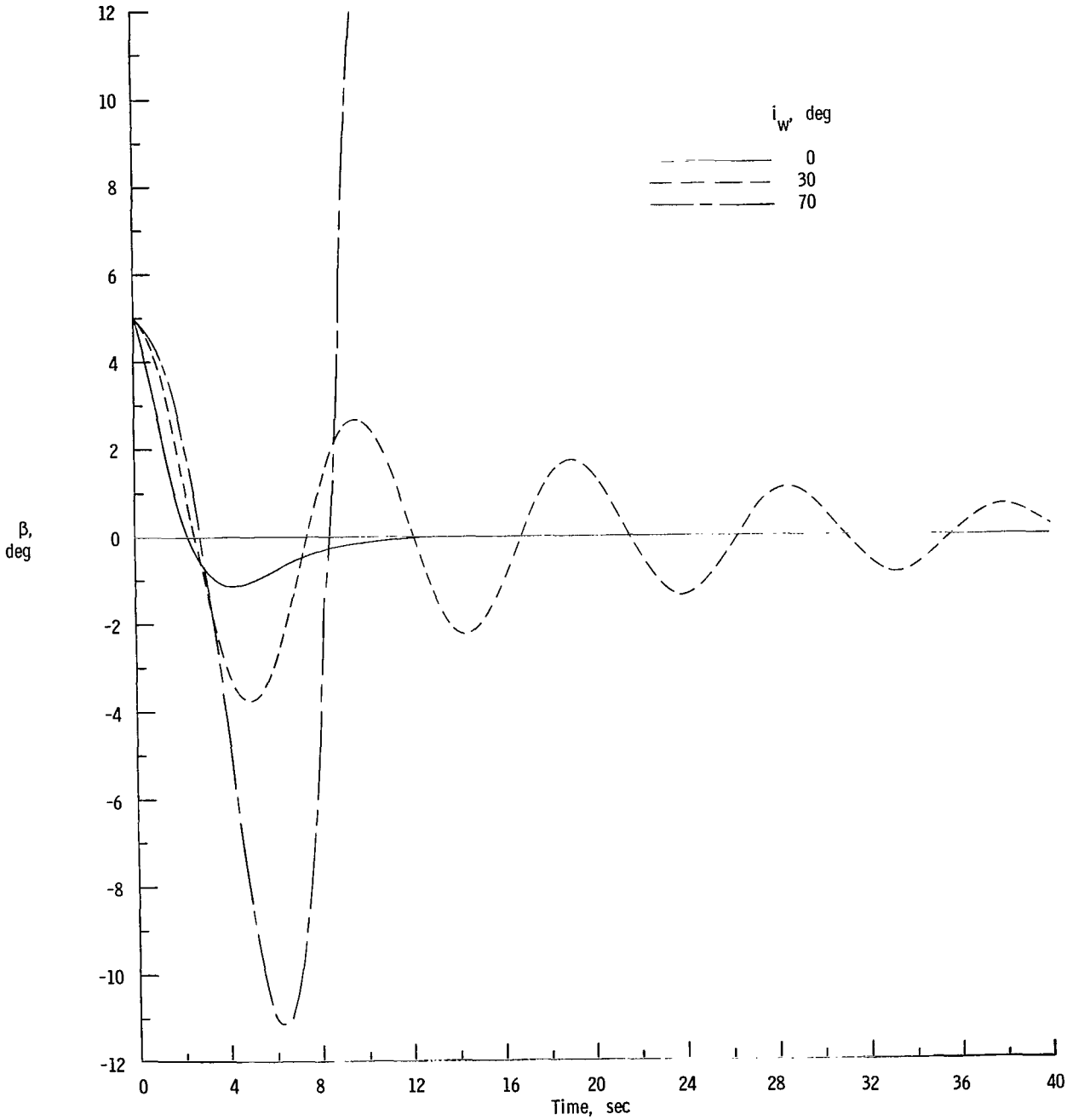

Figure 16.- Calculated response of full-scale airplane after release from 5^{o} sideslip at several wing-incidence angles.

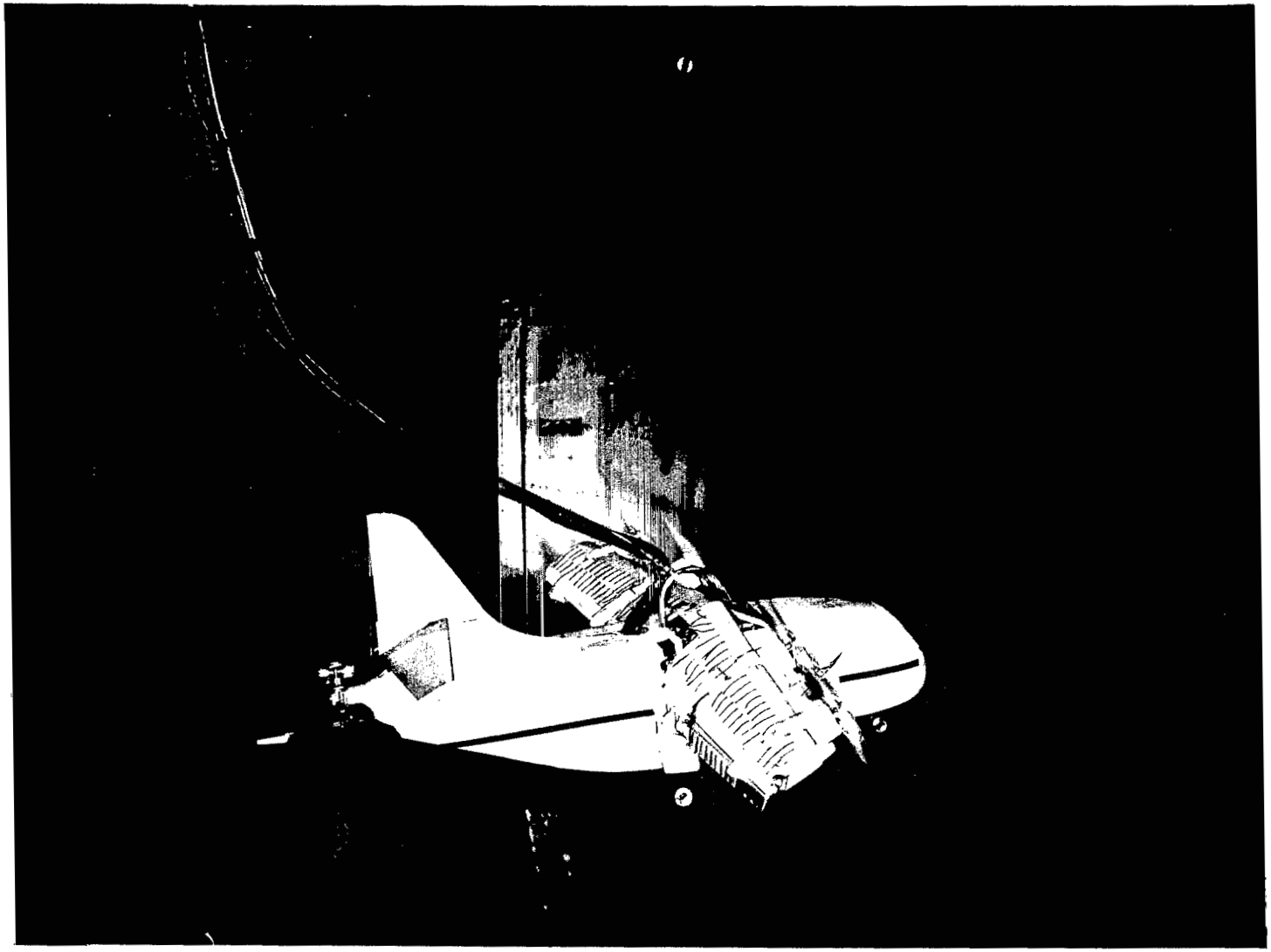

Figure 17.- Photograph of the 1/9-scale model in free flight. L-63-8475

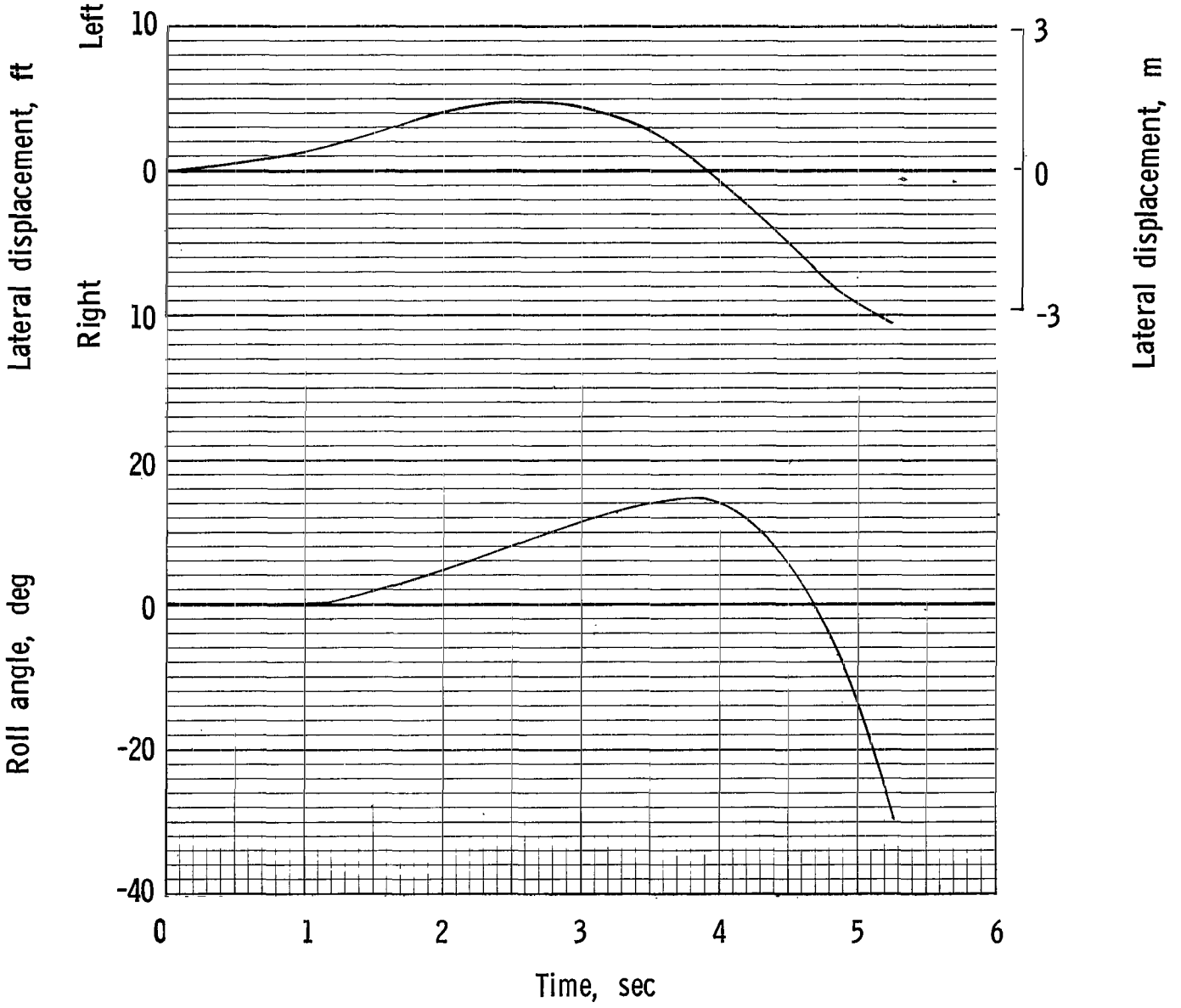

Figure 18.- Control-fixed rolling oscillation of the model in hovering flight out of ground effect.

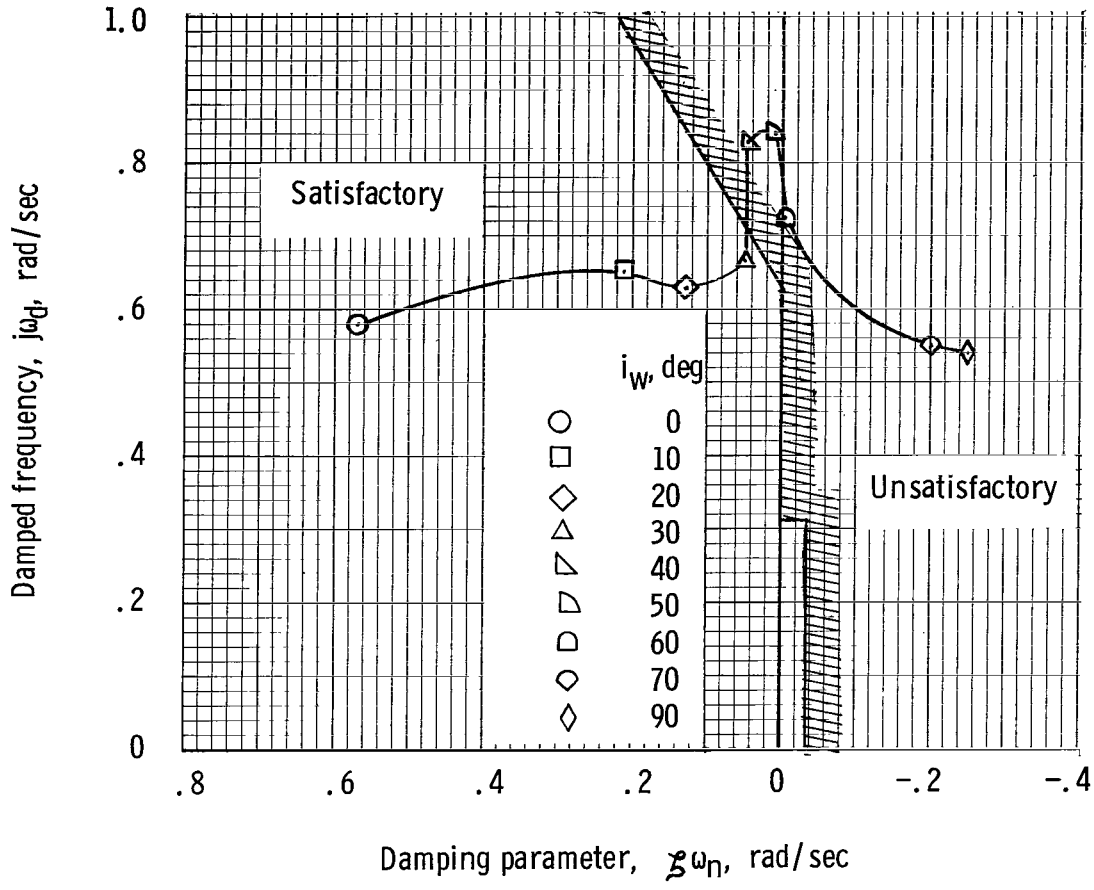

(a) Helicopter requirements.

Figure 19.- Comparison of calculated results with current handling quality requirements.

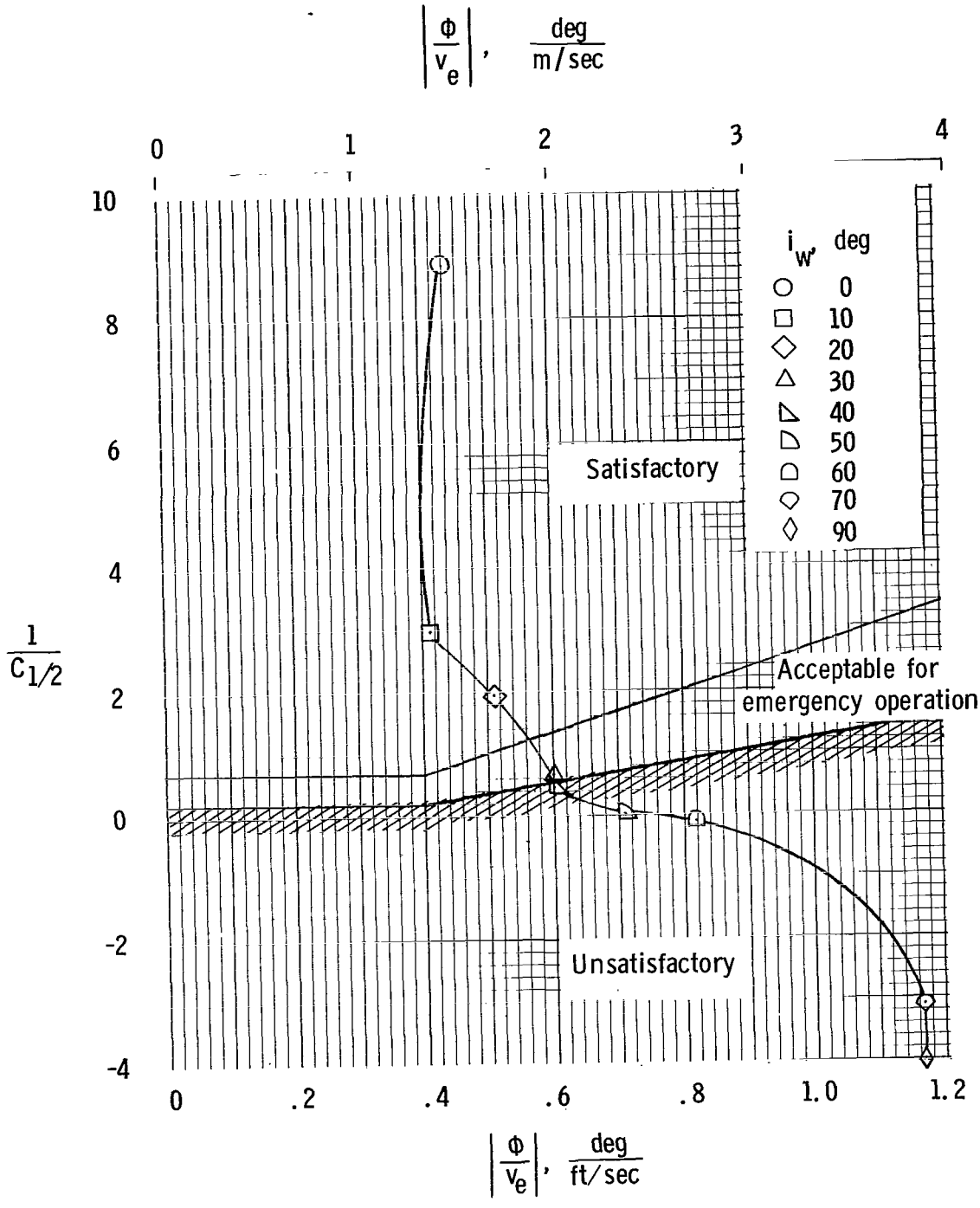

(b) Airplane requirements.

Figure 19.- Continued.

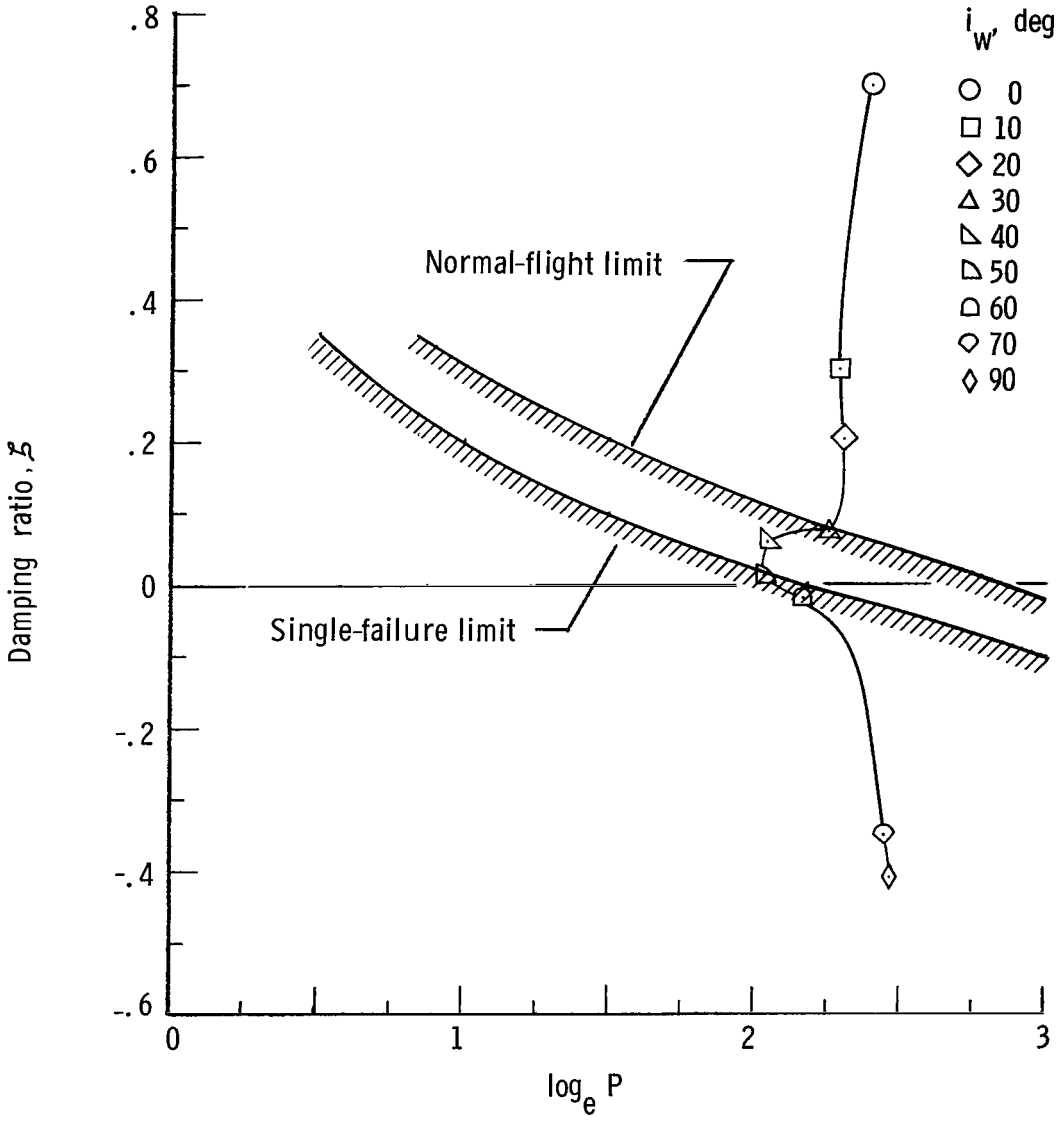

(c) V/STOL airplane requirements.

Figure 19.- Concluded.

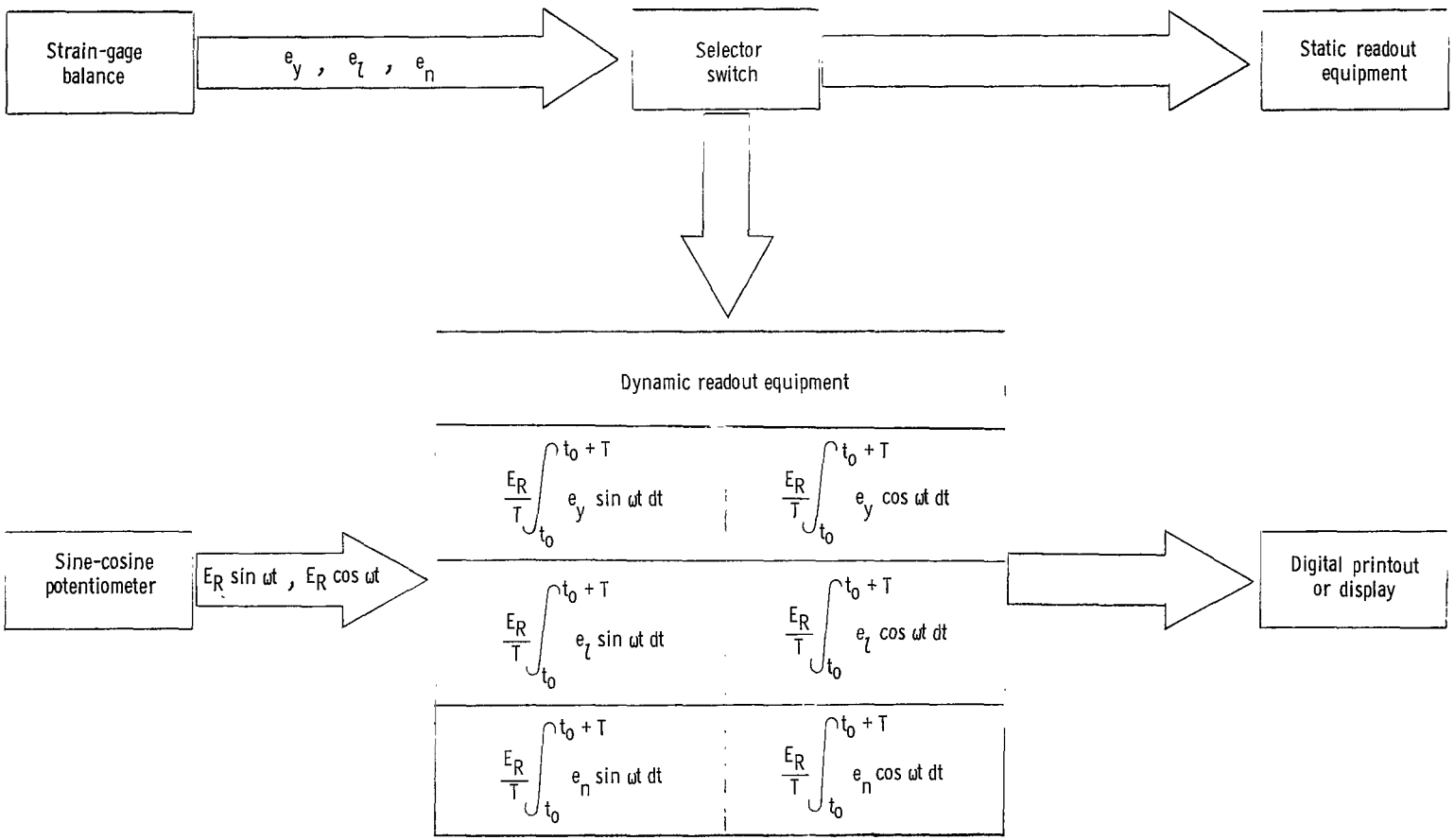

Figure 20.- Schematic diagram of data-reduction system.

"The aeronautical and space activities of the United States shall be conducted so as to contribute . . . to the expansion of human knowledge of phenomena in the atmosphere and space. The Administration shall provide for the widest practicable and appropriate dissemination of information concerning its activities and the results thereof."

—NATIONAL AERONAUTICS AND SPACE ACT OF 1958

NASA SCIENTIFIC AND TECHNICAL PUBLICATIONS

TECHNICAL REPORTS: Scientific and technical information considered important, complete, and a lasting contribution to existing knowledge.

TECHNICAL NOTES: Information less broad in scope but nevertheless of importance as a contribution to existing knowledge.

TECHNICAL MEMORANDUMS: Information receiving limited distribution because of preliminary data, security classification, or other reasons.

CONTRACTOR REPORTS: Scientific and technical information generated under a NASA contract or grant and considered an important contribution to existing knowledge.

TECHNICAL TRANSLATIONS: Information published in a foreign language considered to merit NASA distribution in English.

SPECIAL PUBLICATIONS: Information derived from or of value to NASA activities. Publications include conference proceedings, monographs, data compilations, handbooks, sourcebooks, and special bibliographies.

TECHNOLOGY UTILIZATION PUBLICATIONS: Information on technology used by NASA that may be of particular interest in commercial and other non-aerospace applications. Publications include Tech Briefs, Technology Utilization Reports and Notes, and Technology Surveys.

Details on the availability of these publications may be obtained from:

SCIENTIFIC AND TECHNICAL INFORMATION DIVISION

NATIONAL AERONAUTICS AND SPACE ADMINISTRATION

Washington, D.C. 20546